A multiscale microstructure-based model for the drying shrinkage deformation of cement-based materials

Lin Liu [(1),*], Huisu Chen [(2)] ,Chaojun Wan [(3)] , Mingzhong Zhang [(4)]

[(1)]College of Civil and Transportation Engineering, Hohai University,Nanjing 210098, China

[(2)] Jiangsu Key Laboratory of Construction Materials, School of Materials Science and Engineering,Southeast University, Nanjing 211189, China

[(3)] College of Materials Science and Engineering, Chongqing University, Chongqing 400044, China

[(4)] Department of Civil, Environment and Geomatic Engineering, University College London, Gower Street London, WC1E 6BT, UK.

(1) *Email:liulin@hhu.edu.cn, Tel: +8625 83786183, Fax: +8625 83786183

(2) Email: chenhs@seu.edu.cn

(3) Email: cjwan@cqu.edu.cn

(4) Email: mingzhong.zhang@ucl.ac.uk

Abstract:

This paper presents a multiscale model forthe drying shrinkage deformation of cement-based material by incorporating itscorresponding multiscale computer-generated structure at different scales in a three-dimensional lattice model.Assuming effects of capillary tension and disjoining pressure are the reason for the drying deformation, the water desorption in capillary pores within 100%-to-85% relative humidity (RH) range and that in gel pores within 85%-to-50% RH range are investigated.By considering the contribution of capillary water, gel water as well as interlayer water at microscopic and nanoscopic scales, the drying behaviors of calcium-silicate-hydrate gels, cement paste and mortar are studied by gradually upscaling. Experimental results for the drying shrinkage of cement paste and mortar are utilized to validate the proposed model. Finally, the determination and passing-through of parameters associated with the multiscale model are discussed.

Keywords: Drying shrinkage, water desorption, multiscale model, lattice analysis, capillary pressure

1. Introduction

Drying shrinkage deformation can be a major cause of the deterioration of concrete structures and has been intensively investigated by experiments [1-11] and by simulations [2, 9, 13-17]. In the range of relative humidity (RH) that a typical concrete structure will experience,the drying forces of shrinkage are generally considered as capillary tension and disjoining pressure [11, 15, 18-21]. The

macroscopically observed drying shrinkage deformation of concrete, in principle, is determined by the water existing in calcium-silicate-hydrate (C-S-H) and in the capillary pores of cement paste. For the purpose of exploring the drying nature of cement-based materials, knowledge of the water desorption processes in the nanostructure of C-S-H and in the microstructure of cement paste, of the deformation of C-S-H, of the deformation of cement paste is needed.

In simulation, for a microstructure-based approach, it is a conflict between computing the drying deformation of big size materials (i.e., concrete, on the order of magnitude millimeter to meters) and incorporating the stimulus source at very small size (i.e., water pressure change in the pores on the order of magnitude nanometers) in. In order to solve this problem, multiscale models are proposed. Multiscale models aim to establish a relation between macroscopically observable phenomena and their finer-scale origin [22]. Based on the structure of materials in question at a respective observation scale, the physical/chemical/mechanical/hygro processes within the materials can be considered [23-28] and their effect on the macroscopic material performance can be obtained by means of appropriate upscaling schemes [22, 29-34]. Combining continuum micromechanics with cement hydration models, Pichler C. et al. [22] have proposed a multiscale model to predict the autogenous-shrinkage deformation of cement-based materials. Combining three-dimensional lattice fracture model with material models of C-S-H and cement paste, Liu L. et al. [16] have developed a two-scale model to predict the drying shrinkage of cement paste for high humidity case. Nevertheless, rare modeling work is reported based on a systematic approach including water desorption processes in the nanoscopic and microscopic pores, the response of C-S-H gels and cement paste to the water

desorption at different scales, and the consequent drying shrinkage deformation of cement-based composites. The goal of this paper is to investigate the above issues systematically.

This paper presents a multiscale microstructure-based model topredict the drying shrinkage deformation of cement-based materials. The combined application of a multiscale material modeland a three-dimensional (3D) lattice model makes it possible to study the drying behaviors of C-S-H gels, cement paste and mortar by gradually upscalingand by incorporating the contribution of capillary water, gel water as well as interlayer water. Assuming effects of capillary tension and disjoining pressure are the main reason for the drying deformation of cement-based materials, the water desorption in capillary pores within 100%-to-85% RH range and that in gel pores within 85%-to-50% RH range are investigated.Experimental results for the drying shrinkage of cement paste are utilized to validate the proposed model. The determination and passing-through of parameters associated with the multiscale model are finally discussed.

2. Capillary pressure and disjoining pressure

In general agreement, changes in capillary pressure, disjoining pressure and the surface tension of solid particles are assumed as mechanisms governing drying shrinkage. Whether a particular mechanism is active is dependent on the internal relative humidity (RH) within the material.

(a) At high humidity (100%-to-85% RH), moisture loss occurs in capillary pores and gel pores remain full of water [11, 35]. Effects of capillary pressure and disjoining pressure are active [15, 20].

(b) At mid humidity (85%-to-45% RH), moisture loss occurs in gel pores and only a small amount of liquid water exists in capillary pores [16, 35]. Effects of capillary pressure and disjoining pressure are still active [11, 15, 20].

(c) At low humidity (below about 40%~45% RH), capillary menisci are not stable and the effect of capillary pressure is not present [20]. Effects of disjoining pressure and surface tension of solid particles are active [15, 18, 20].

Recently, Jennings H.M. et al. argued that the effect of surface tension of solid particles may below 20%~25% RH [11, 17]. Normally, the capillary pressure mechanism and the disjoining pressure mechanism are assumed to be predominant because the internal RH of a typical concrete structure will experience intermediate to high humidity [20]. Figure 1 illustrates the geometrical presentation of disjoining pressure zone and capillary pressure zone in a liquid bridge between two spherical substrates.

According to ***Kelvin equation***, the relation between capillary pressure $p_{cap}$and relative humidity is given by[19],

$$p_{cap} = p_{atm} - p_L = -\frac{RT}{\bar{V}_L}\ln h_R \qquad (1)$$

where$p_L$is pressure in pore fluid, MPa; p_{atm} is the atmospheric pressure, MPa; $\bar{V}_L$ is the molar volume of water,cm^3/mol; R is the universal gas constant,J/(mol•K); $T$is temperature, K; $h_R$is the value of relative humidity.According to ***Laplace equation***, the relation between capillary pressure p_{cap} and the water-vapor menisci can be written as [19],

$$p_{cap} = \gamma_{LV}\kappa_{LV} \quad (2)$$

where γ_{LV} is the surface tension of the liquid/vapor interface, J/m^2; κ_{LV} is the curvature of the liquid/vapor interface, μm^{-1}. Based on a spherical meniscus, combing equation (1) and equation (2), ***Kelvin-Laplace equation*** can be obtained, described as [19],

$$r_{\Delta u} = -\frac{2\gamma_{LV}}{(RT/\bar{V}_L)\ln h_R} \quad (3)$$

where $r_{\Delta u}$represents the smallest pore access radius of the pore volume currently invaded by air, that is, pore radius threshold for drying at a specific h_R and T.At 293.15K, we have R=8.314J/(mol•K), $\bar{V}_L$ =18.032cm^3/mol and γ_{LV}=0.072 J/m^2[36]. At 50% RH, the radius $r_{\Delta u}$ equals to 1.5 nm and at 85% RH, the radius $r_{\Delta u}$ equals to 6 nm.

The disjoining pressure is active in areas of hindered adsorption, i.e. where the distances between the solid surfaces are smaller than two times the thickness of the free adsorbed water layer [18], see figure 1.It is not possible to quantify the absolute disjoining pressure. However, the change in disjoining pressure can be quantified using the Kelvin-Laplace equation since the change in stress of the absorbed water must be the same as the change in stress for the evaporable water [20]. Therefore, at above 45% RH, the Kelvin-Laplace equation accounts for both the shrinkage stress associated with the surface tension and the disjoining pressure mechanisms [20]. Jennings H.M. et al. indicatedthe same point but modify the active range of Kelvin-Laplace equation into 25%-100% RH[11]. Take the atmospheric pressure p_{atm}equals to zero as reference, the stimulus stress for drying can be considered as a negative pressure of liquid water $p_{L,}$ which can be obtained according to Kelvin equation.

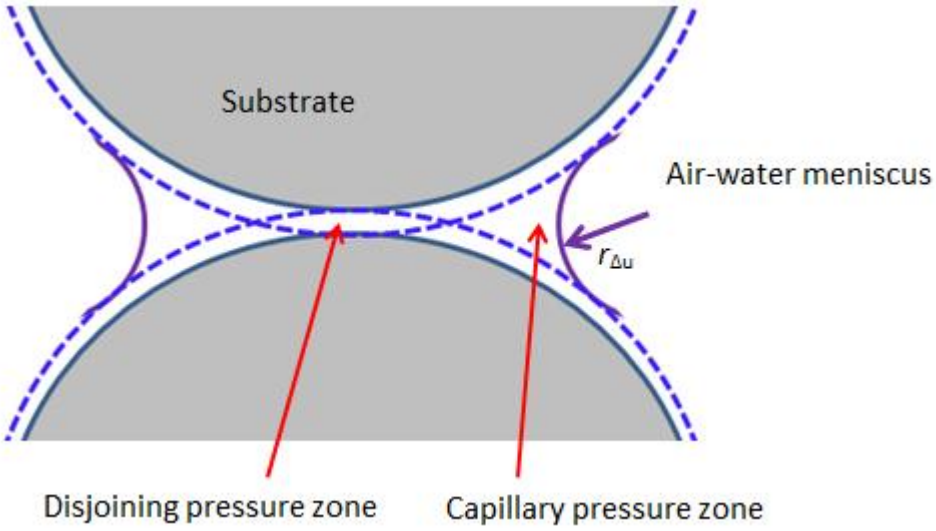

Figure 1: Geometrical illustration of capillary adhesion and disjoining pressure zones.

3. Multiscale structure model for cement-based materials

Cement-based material manifestsitself heterogenous at different scales [22, 29-30,32]. According to the problems dealt with, the smallest scale to be considered can be different. With regard to the drying issue, in a normal RH range, moisture loss may occur in gel pores and capillary pores, while the water in non-empty pores determinates the drying deformation. Table1 summaries the pore empty processes and the contribution water to the drying deformation of cement-based materials at different RH. Therefore, the cement-based material need be refined to a scale where the smallest characteristic phase, i.e., interlayer water, can be incorporated in. For the purpose of drying processes simulation and shrinkage deformation analysis, figure 2 illustrates how we categorize the multiscale microstructures of cement-based material. The C-S-H is analyzed at two levels. At level 0, globule level (10^{-10}~10^{-8} m), the drying deformation attributed to interlayer water can be taken into account.

At level 1, C-S-H gels level (10^{-9}~10^{-7} m), the empty process of gel pores can be characterized and the drying contribution of gel water can be quantified. Similarly, at level 2, cement paste (10^{-6}~10^{-4} m) level, the empty process of capillary pores can be characterized and the drying contribution of capillary water can be quantified. By incorporating the drying deformation of cement paste predicted at cement paste level in the simulation about mortar or concrete at level 3, , the drying deformation of mortar or concrete (10^{-5}~10^{-1} m) can be obtained.

Table 1: A summary of pore empty processes [11] and contribution water to the drying deformation.

Relative humidity (RH, %)	Water desorption process	Contribution water to the drying deformation
100-to-85	Capillary pores empty by a pore blocking mechanism.	Capillary water LD-gel water HD-gel water interlayer water
85-to-50	LD-gel pores empty by pore blocking.	LD-gel water HD-gel water interlayer water
50-to-25	HD-gel pores continue to empty by pore blocking.	HD-gel water interlayer water

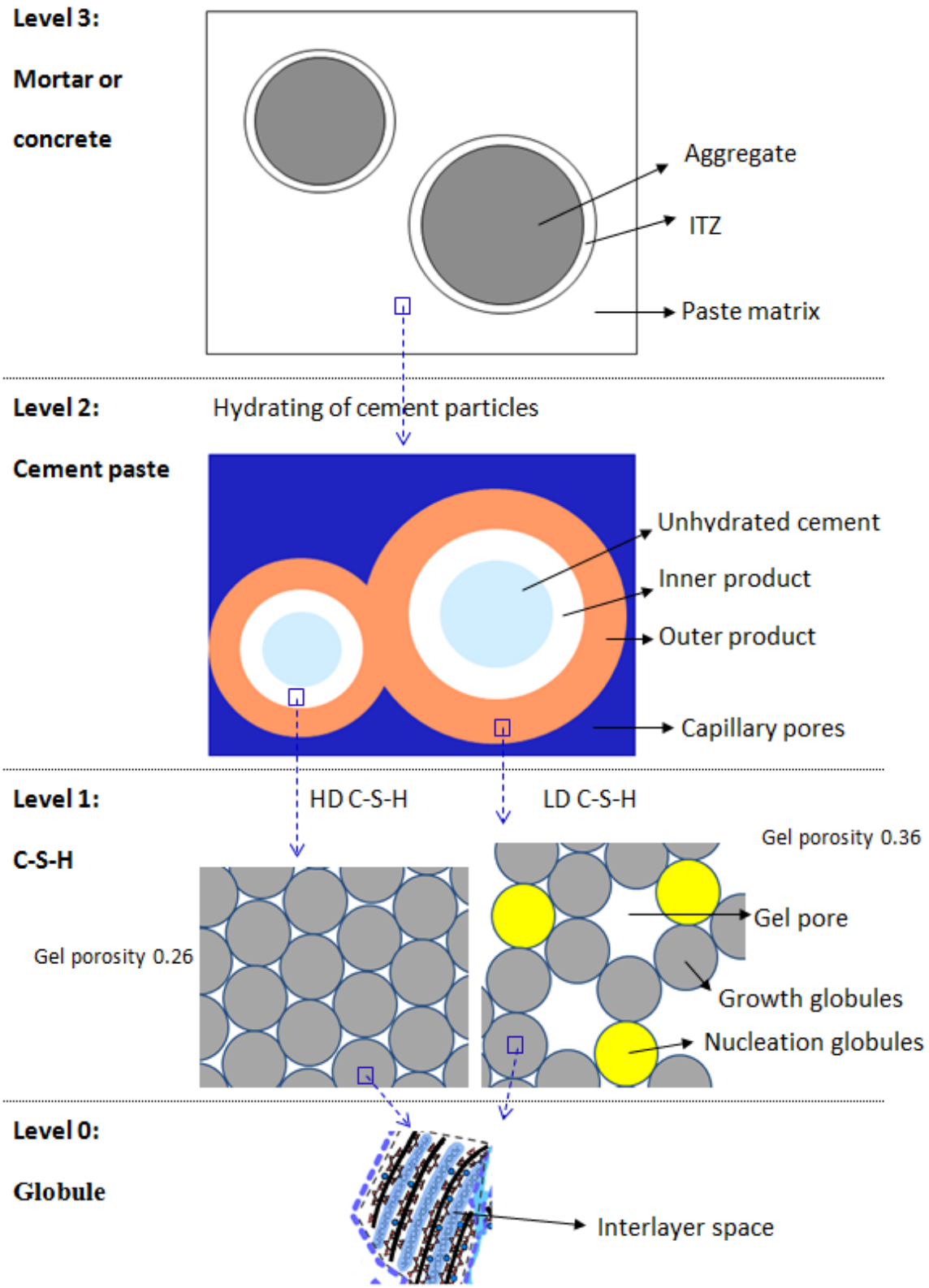

Figure 2: Multiscale structure of cement-based materials [11, 16].

3.1 Calcium-silicate-hydrate at nanoscopic scale

3.1.1 Concept models of C-S-H

A number of concept models for describing the structure of C-S-H have been proposed, including layered models, crystal-like models, colloidal models, fractal models and so on [37]. Two types of C-S-H with different densities in terms of high density C-S-H (HD C-S-H or HD gel) and low density C-S-H (LD C-S-H or LD gel) are acknowledged, and theirgel porositiesare approved to be 0.26for HD gel and 0.36for LD gel [30,38-39]. At the scale between 1 and 100 nm, evidence suggests that C-S-H behaves like a colloidal precipitate [40-41]. Jennings H.M. and his co-workers have proposed a granular model assuming that the HD and LD gels are formulated by colloids flocculation [35, 39, 42].

3.1.2 Particle packing model of C-S-H gels

Continuing to the colloidal concept model and experimental evidence, particle packing models of HD and LD gelshavebeen established to investigate its various properties [16, 43-44].According to the particle packing model of HD C-S-H, a regular assembly of globulesof 5 nm in diameter is performed and the packing fraction of globules 0.74 is guaranteed. Both hexagonal close packing (HCP) and face-centered cubic packing (FCC) can provide a packing density of 0.74. The former is employed in this study.

According to the particle packing model of LD gel, a random hexagonal closepacking(RHCP) arrangement is performed as the following procedures: First, a number of globulesof 5 nm in diameter are randomly created by Monte-Carlo algorithm in a 3D space, called ‘nucleation globules’. Second, new globules with the same size randomly grow from the ‘nucleation globules’ following a HCP arrangement until the packing fraction of globules is 0.64. See illustrations in figure 2. With a length of 100 nm, 12489 and 10469 globules are respectively generated for HD and LD C-S-H, given in figure 3.

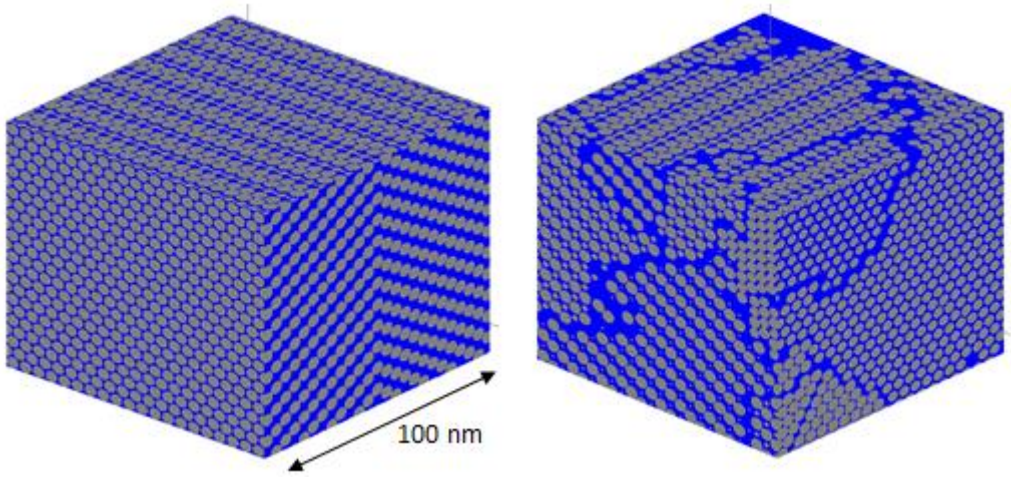

Figure 3: 3D images of nanostructures of HD-gel (left) and LD-gel (right).

3.1.3The structure of globules

The concept of “globule” was proposed in the granular model for describing the structure of two types of C-S-H gels [40]. It can also be called C-S-H particles and represent the solid part of C-S-H gels excluding gel pores [42]. There are mainly two assumptions about the structure of the C-S-H

particle, layer-like or granular-like. According to the granular model, a globule is a basic cluster composed of hexagonal close packing blocks those are the basic unit [40].The water between these basic blocks can be assumed as interlayer water. Irrespective of the type of C-S-H gels, a nanoporosity of 0.18 of a globule filled by structural water is manifested [30]. According to the layer-like theory, the nanoscale C-S-H particle is composed of calcium silicate sheets with OH^- and interlayer space with physically bound water (i.e., interlayer water)[11, 42].The interlayer water is associated with disjoining pressure and removal of water from the interlayer spaces causes partial collapse of the globule[11].

In this study, the globule is assumed to be composed of C-S-H solid and interlayer water. The interlayer water phase is randomly distributed in the C-S-H solid with a volume fraction of 0.18. The contribution of interlayer water to the drying deformation of globules will be discussed in section 5.

3.1.4Characteristics of gel pores

Jennings H.M. divided gel pores into three categories: (1) the interlayer gel pore (IGP) with size ≤ 1 nm; (2) the small gel pore (SGP) between 1~3 nm; (3) the large gel pore (LGP) between 3~12 nm [35], and further clarified gel pores are those in the range of 2~8 nm [11].By virtual of the particle packing models for C-S-H gels, the gel pore size distributions can be obtained. For HD gel, attributed to the regular arrangement of globules, the SGP less than 3 nm across is predominant, and no LGP is

found, see figure 4. This is in agreement with the division of 50% RH as mentioned in table 1, below which HD gel pores start to get empty.

For LD gel, both SGP and LGP exists, see the gel pore size distribution curves in figure 5. Calculations are performed on five LD gelstructures with side length of 100 nm, 150 nm, 200 nm, 300 nm and 400 nm and designated as GS100, GS150, GS200, GS300 and GS400. The gel pore size distribution becomes reproduciblewhen the side length of structures is no smaller than 150 nm. Hereafter, the nanostructure of LD gel with side length of 150 nm is utilized.In addition, it is found that the SGP porosity is about 0.17, while the LGP porosity is about 0.09 in LD gel. The majority pores are between 2~5 nm. It indicates that an obvious gas-liquid phase change will occur in LD gel below 65% RH (corresponding to the 5 nm width pore), and that gel pores in LD gel continue to get empty below 50% RH where HD gel pores are supposed to get empty.

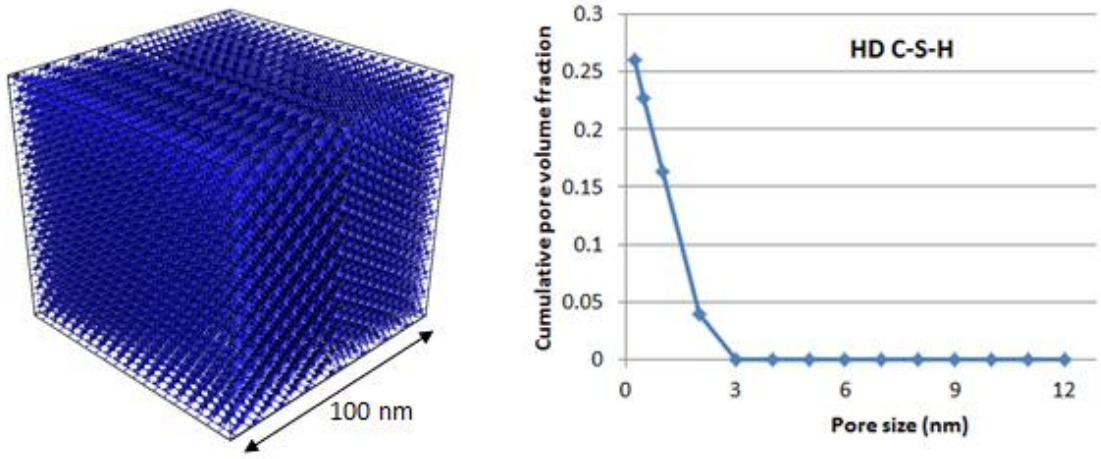

Figure 4:Pore structure (left) and poresize distribution (right) of HD-gel.

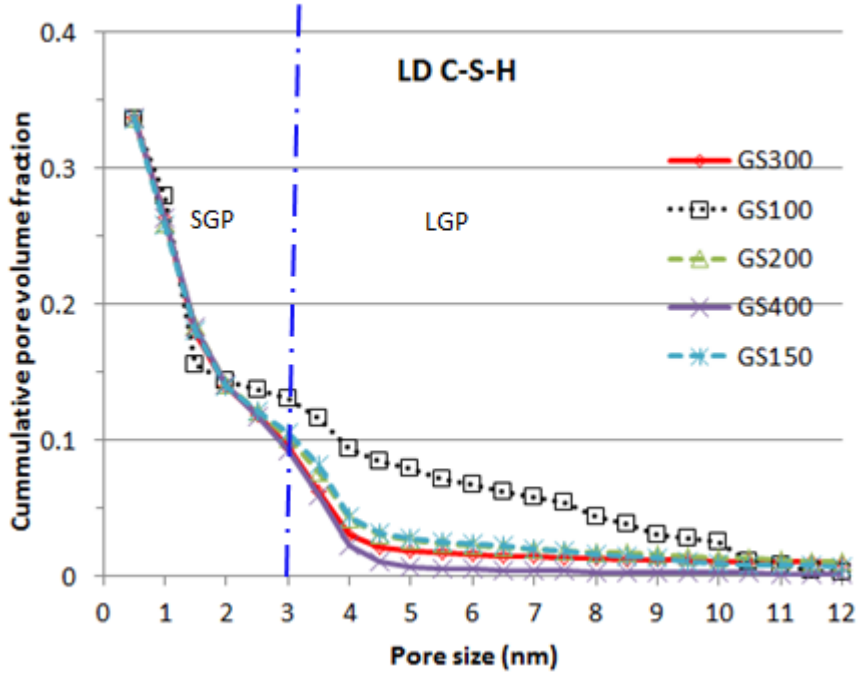

Figure 5:Simulated gel pore size distribution of LD C-S-Hwith various side lengths.

3.1.5Gas-liquid phase changes in LD C-S-H

According to equation (3), at 85% RH, pores with size larger than 12 nm get empty, whileat 50% RH, pores with size larger than 3 nm can get empty. After digitalize the structure of LD-gel into a voxel-represented structure with a high resolution, the water desorption process in LD-gel pores can be configured, see figure 6. Attributed to the small scale of HD-gel pores, as shown in figure 4, HD-gel pores remain full of water at 50% RH above.

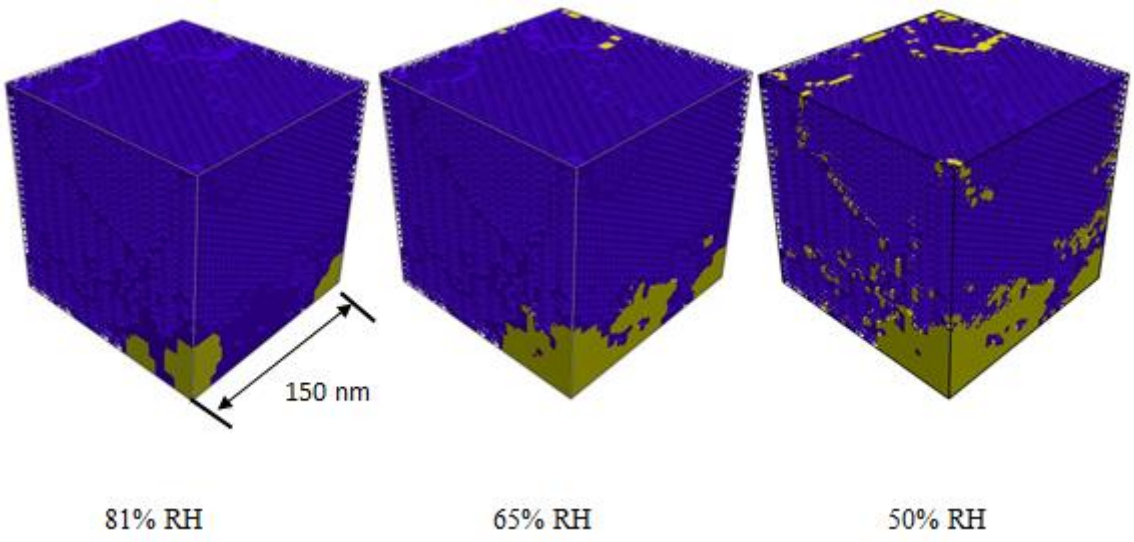

Figure 6: Changes of gas-liquid phase in LD-gel as RH decreases (yellow: air; blue: water) (Displayed at a resolution of 0.5 nm/voxel).

3.2 Cement paste at microscopic scale

3.2.1 Microstructure model of cement paste

Both experimental techniques such as X-ray micro-tomography (micro-CT) [34, 45-46] and focused-ion beam nanotomography (FIB-nt) [47-49] and computer models, i.e., HYMOSTRUC3D [50-51], CEMHYD3D [52], µic [53], etc., can provide the 3D microstructure of cement paste. In this study, the HYMOSTRUC3D model is utilized to obtain the microstructure of cement paste at microscopic scale,and for comparison, a cement paste with the same material parameters from micro-CT scan with a resolution of 0.5 µm/voxel provided by UIUC is utilized.

According to HYMOSTRUC3D, cement particles are modeled as digitized spheres randomly distributed in a 3D body with a periodic boundary condition. The hydrating cement grains are

simulated as growing spheres. The hydration products, in terms of inner and outer hydration product, are formed around the grain. It is assumed that the inner hydration product is constituted of high density C-S-H, and the outer hydration product is mainly constituted of low density C-S-H and calcium hydroxide (CH). Material parameters for cement paste with water-to-cement ratio (*w/c*) 0.5 are listed in table 2. For cement paste of water-to-cement ratio (*w/c*) 0.5 after hydrating 28 days, according to the HYMOSTRUC3D model, degree of hydration is 0.75. 3D images of cement paste obtained by micro-CT and by the HYMOSTRUC3D modelare illustrated in figure 7.Volume fractions of hydration products of cement paste by HYMOSTRUC3D and by micro-CT are listed in table 3. The content of hydration products by HYMOSTRUC3D is generally in consistent with that by micro-CT. Due to some technical limitations, the HD-gel and LD-gel can not be particularly distinguished from hydration products in the microstructure of cement paste by micro-CT.

Table 2: Material parameters utilized in the HYMOSTRUC3D model for cement paste.

Cement type	Portland CEM I 42.5N
Mineralogical composition of cement	64% C_3S, 13% C_2S, 8% C_3A, 9% C_4AF by mass
Fineness (Blaine surface area value) of cement	420 m^2/kg
Minimum diameter of cement particle	1 μm
Maximum diameter of cement particle	37 μm
Size interval of cement particles	1 μm
Water-to-cement ratio	0.5

Table 3: Volume fractions of hydration products of cement paste by HYMOSTRUC3D and by micro-CT(Computed at a resolution of 0.25 μm/voxel for HYMOSTRUC3D and 0.5 μm/voxel for micro-CT).

	Unhydrated cement	Inner product	Outer product	Capillary pore
By HYMOSTRUC3D	0.095	0.289	0.412	0.204
By micro-CT	0.102	0.711		0.187

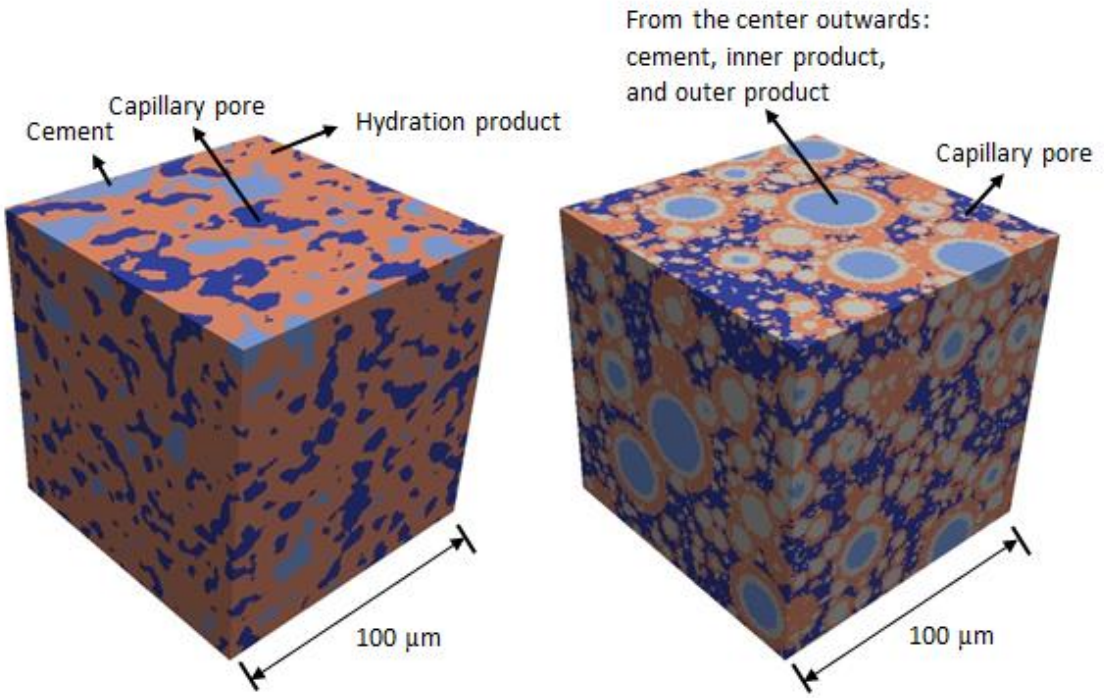

Figure 7: 3D images of microstructures of cement paste (CEMI 42.5R, *w/c* 0.5, 28 days). Left:cement paste by Micro-CT; Right:cement paste by HYMOSTRUC3D.

3.2.2 Characteristics of capillary pores

Mindess S. and Young J.F. defined capillary pores as pores with diameter ranging from 10 nm to 0.5 μm [54]. Jennings H.M. pointed out that the difference between capillary pores and gel pores was that capillary pores can get empty while gel pores won't when above about 85%RH [35]. Adoptingthe latter division, the division size between gel pores and capillary pores is about 12 nm according to Kelvin-Laplace equation. Recently, Jennings H.M. defined that capillary pores are those poreswith width between about 8 nm and 10 μm and responsible for the drying behavior above 85% RH [11]. In this study, capillary pores we concerned are those pores in the microstructure of cement paste at microscopic scale and can get empty above 85% RH.

Figure 8 shows the capillary pore size distribution in cement paste when the side length of cement pasteis 75μm, 100μm, 150μm and 200μm, and designated as PS75, PS100, PS150 and PS200, respectively.The total capillary porosity in cement paste with side length of 75 μm is obviously lower than others, and the pore size distribution curves are highly consistent when the side length of cement paste is no smaller than 100 μm. Therefore, cement paste with side length of 100 μm is utilized in the following simulations.

Incorporating the pore size distributions of gel pores in HD and LDgels analyzed in section 3.1 in that of capillary pores shown in figure 8, the pore size distribution curve of cement paste covering gel pores and capillary pores can be quantified by simulation, see figure 9. For comparison, a curve

by mercury intrusion porosimetry (MIP) from literature [51] is plotted. There is obvious discrepancy between the simulated curve and the MIP test one. Within capillary pores range, the cumulative pore volume by simulation is larger than that by MIP test. While within gel pores range, the cumulative pore volume by simulation is lower. This discrepancy may attributed to (i) some basic assumptions of HYMOSTRUC3D model, i.e., spherical cement particles and the minimum size of cement particle; (ii) test limitations of MIP, i.e., the "ink-bottle" effect and the microstructural change during sample preparation. More discussions about the reasons for pore size distribution discrepancy of cement paste between HYMOSTRUC3D simulation and MIP technique can be found in literature [24, 51]. Although the simulation about pore size distribution doesn't show highly consistent with experimental result, reliable predictions in mechanical and diffusion properties were obtained in previous studies [24-25, 33]. Therefore, it is necessary to compare the predicted drying shrinkage of cement paste by simulation with that by experiment, this will be discussed in section 5.2.

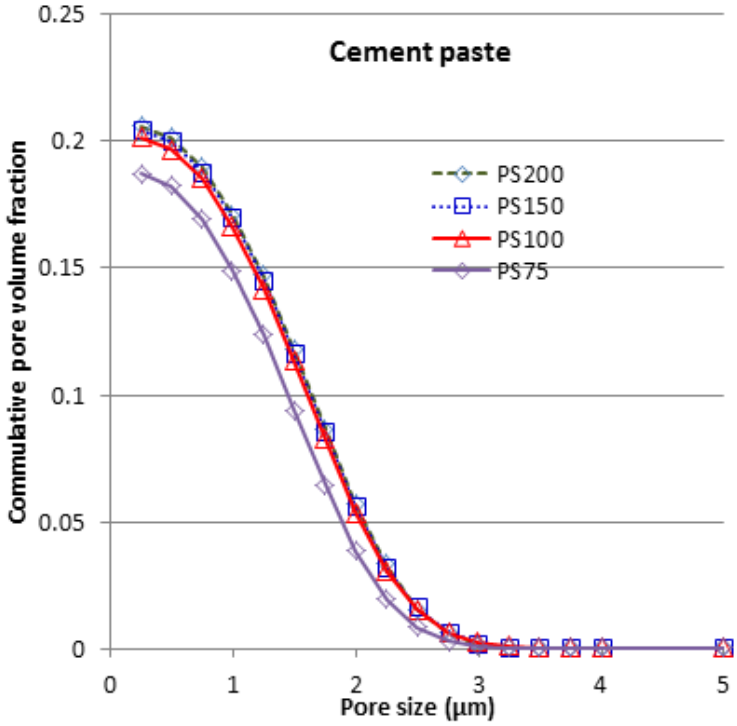

Figure 8: Simulated capillary pore size distribution of cement paste from HYMOSTRUC3D.

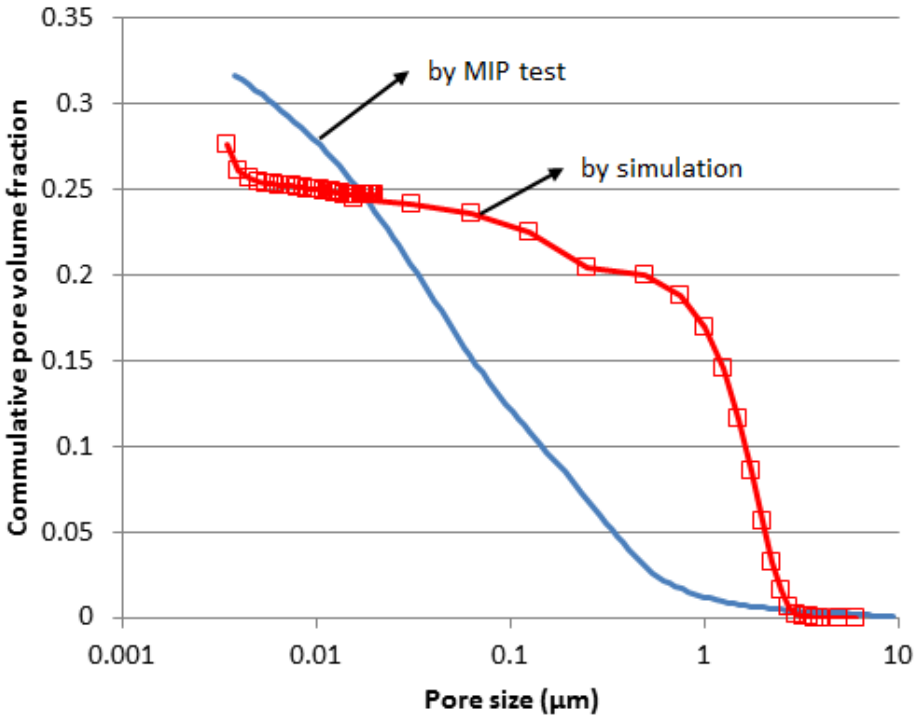

Figure 9: Pore size distribution curves of cement paste (CEMI 42.5R, *w/c* 0.5, 28 days) by simulation and MIP test [51].

3.2.3Gas-liquid phase changes in cement paste

Within the range 100%-to-85% RH, apparent gas-liquid phase transition takes place in capillary pores.Based on Kelvin-Laplace equation and the microstructure model of cement paste, Liu L. et al. configured the gas-liquid phase in capillary pores [16], and demonstrated that only a small amount of liquid water exists in capillary pores below 85% RH,see figure 10.

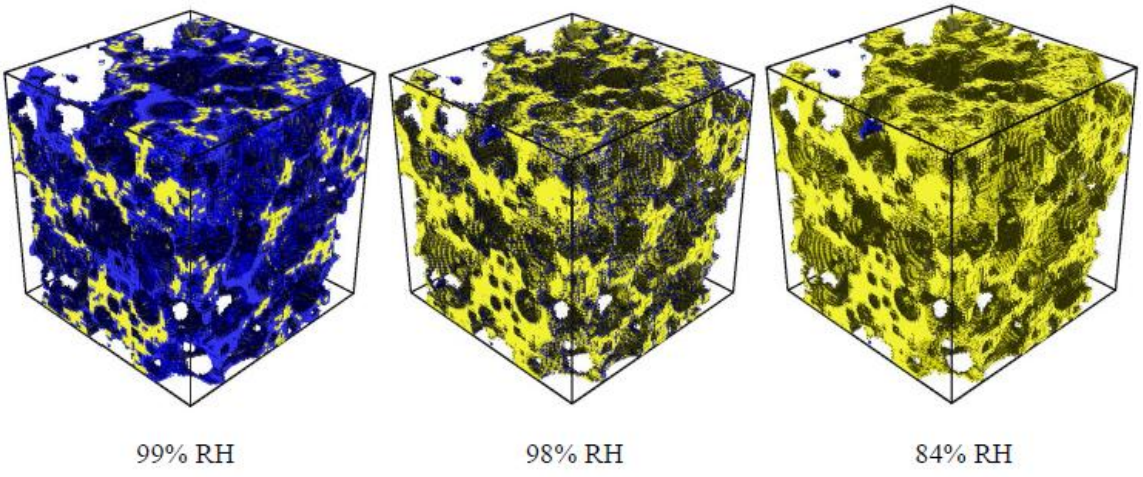

Figure 10: Gas-liquid phase in the pore structure of cement pasteunder different RH (yellow: air, blue: water. Capillary pores larger than 10 nm are illustrated). [16]

3.3Concrete/mortar at mesoscopic scale

At mesoscopic scale, concrete/mortar is usually considered as composites of paste matrix, aggregate and interfacial transition zone (ITZ). For simplicity, a spherical particle packing model is usually

utilized to generate the mesostructure of mortar/concrete, where spherical particlesrepresent sands/aggregates. Assume the sand particles satisfy with Fuller's distribution, the mortar mesostructures with different sample sizes (5 mm, 6 mm, 8 mm and 10 mm) are generated using the spherical particle packing model, where the sand volume fraction (V_{agg}) is 0.46, the maximum and minimum diameter of sand (D_{max} andD_{min}) are 2.0 mm and 0.2 mm, and the size interval of sand 0.2 mm. The sand size distribution curves with different sample sizes of mortar designated as MS5, MS6, MS8 and MS10 are given in figure 10. It is found that the sand size distribution curves achieve highly consistent when the side length of mortar is no smaller than 6 mm. An image of the mesostructure of mortar with side length of 6 mm is illustrated in figure 12. In the following simulations, mortar with side length of 6 mm is utilized.

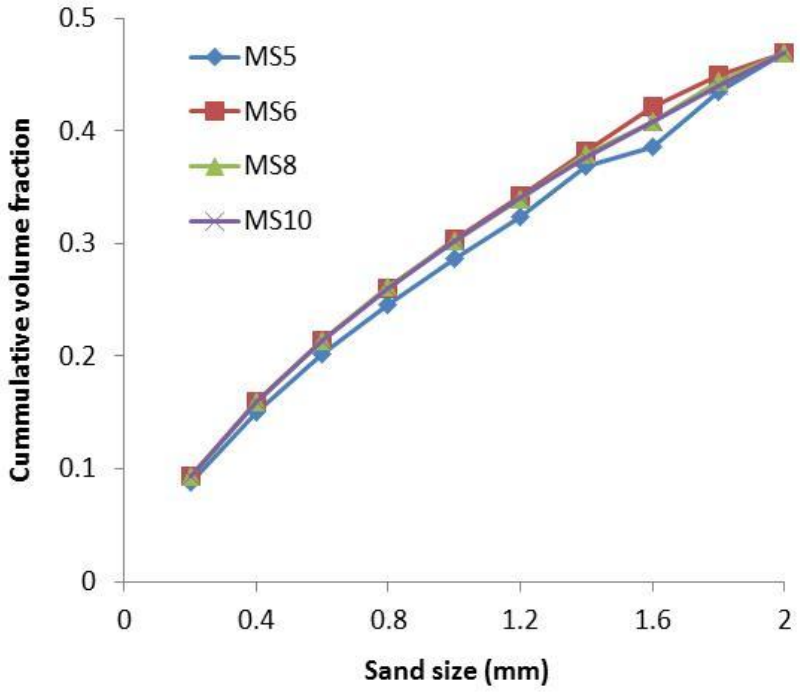

Figure 11: Sand size distributions of mortar (V_{agg}=0.46; D_{max}=2.0 mm; D_{min}=0.2 mm).

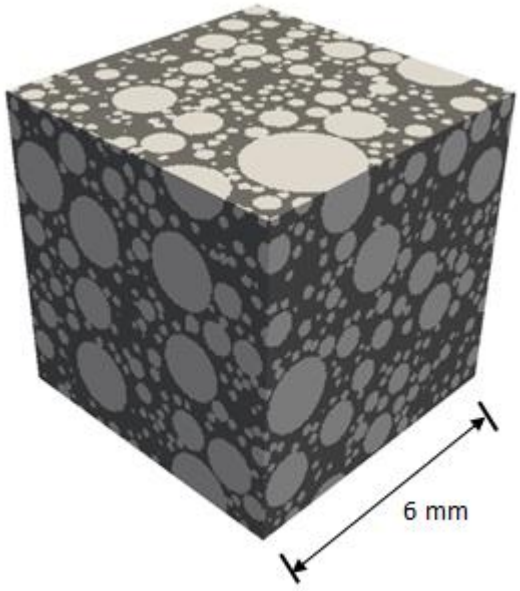

Figure 12: Mesostructure of mortar (Dark: paste matrix; white: sand. V_{agg}=0.46; D_{max}=2.0 mm; D_{min}=0.2 mm).

4. Modeling strategy and three-dimensional lattice analyses

After the multiscale material model has been developed and the water desorption progresses in capillary and gel pores are clarified, the next step is to compute the drying deformation of cement-based materials by applying responsible loads at the respective scale.

4.1Modeling strategy for drying deformation

Based on the multiscale material model described above, the **modeling strategy** is: (1) At C-S-H globule level, to quantify the drying deformation of C-S-H globules attributed to interlayer water. (2) At C-S-H gel level, to characterize the water desorption processes in gel pores and to investigate its

effects on the deformation of C-S-H gels, where the drying deformation of C-S-H globules obtained from the finer scale is utilized. (3) At cement paste level, to characterize the water desorption in capillary pores and to computer the drying shrinkage deformation of cement paste where the deformations of C-S-H gels obtained at C-S-H gel level areutilized. (4) At mortar level, from the mesostructure of mortar, to compute the drying shrinkage deformation of mortar where the deformation of paste matrix obtained at cement paste level is utilized. At each respective scale, the drying deformation of cement-based materials is computed by three-dimensional (3D) lattice model.

Lattice model can be utilized to analyze the deformation and fracturing process of a material in question introduced by external loading [33, 55-56] or internal physical and chemical actions [23, 26-27]. The modelling procedures of lattice model can be generally described as generation of lattice network, imposition of internal or external loads, and computation of stress and strain distribution. The deformation and fracture of the material can be analyzed from the computed stress and strain distribution.

4.2 Generating 3D lattice network

The lattice network construction can be quadrangular, triangular, and irregular geometries [33, 56-57]. Lattice network construction by a quadrangular approach is employed in this study and illustrated in figure 13.The sketch at left side is shown in 2D, and the mesh method also works for 3D case. A network of cells is required first, and a sub-cell is defined within each cell.The side

length ratio of sub-cell to cell is defined as randomness. The cell is distinguished as solid phase and non-solid phase. For solid phase cells, a lattice node is randomly generated within its sub-cell and is responsible for carrying loads. For non-phase cells, for example, gel pore phase in C-S-H gels at nanoscopic scale and capillary pore phase in cement paste at microscopic scale, within which no lattice node is generated. In this case, the network of cells is the voxel-represented structure at different scales. Then, the lattice nodes in the neighboring cells are connected by lattice beam elements. The lattice network system is eventually formed by connection of lattice elements, and is able to carry loads.Based on the materials we concerned at different scales, the network of lattice elements at each respective scale can be constructed. The specification of lattice networks is given in table 4.

The local mechanical properties (Young's modulus $E_{i\text{-}j}$, shear modulus $G_{i\text{-}j}$and tensile strength $f_{i\text{-}j}$) assigned to each element are determined by those of its connecting cells.

$$E_{i-j} = \frac{2}{\frac{1}{E_{\mathrm{n},i}} + \frac{1}{E_{\mathrm{n},j}}} \tag{4}$$

$$G_{i-j} = \frac{2}{\frac{1}{G_{\mathrm{n},i}} + \frac{1}{G_{\mathrm{n},j}}} \tag{5}$$

$$f_{i-j} = \min(f_{\mathrm{n},i}, f_{\mathrm{n},j}) \tag{6}$$

where $E_{i\text{-}j}$, $G_{i\text{-}j}$ and $f_{i\text{-}j}$ represent the Young’s modulus, shear modulus and tensile strength of element connecting node *i*and node *j*. The tensile strength of element is useful in lattice fracture model and

can be neglected in calculations for volume deformation without fracturing. Table 5 lists the mechanical parametersof solid phases in cement-based materials at different scales.

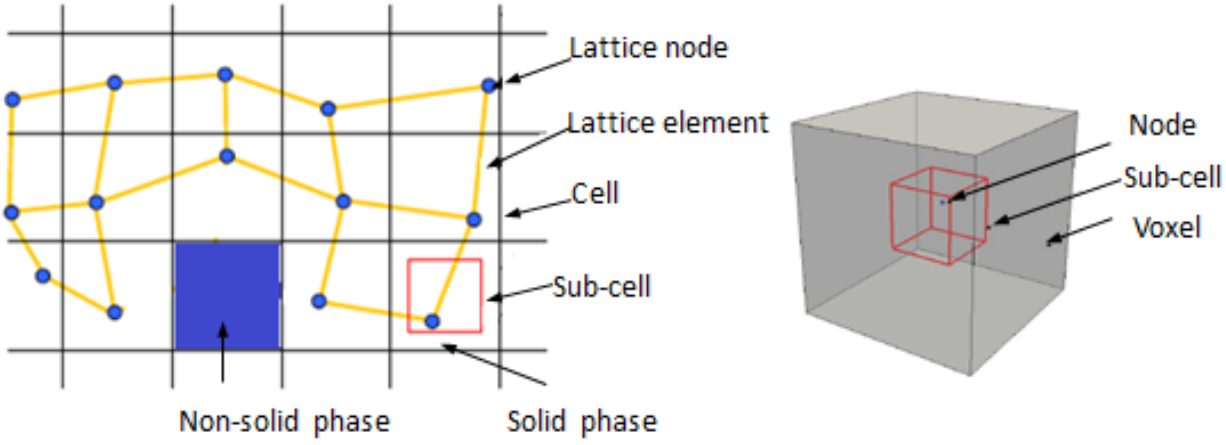

Figure 13: Lattice network construction by a quadrangular approach (reproduced after [33]).

Table 4 Specification of lattice networks

Material scale	Composition phases	Mesh size	Specimen size
Globule level	C-S-H solid and interlayer water	0.1 nm	5 nm × 5 nm × 5 nm
C-S-H gel level	Globule and gel pore	1 nm	100 nm × 100 nm × 100 nm (HDgel) 150 nm × 150 nm × 150 nm (LDgel)
Cement paste level	Cement, inner product, outer product and capillary pore	1 μm	100 μm × 100 μm × 100 μm (HYMOSTRUC3D structure)
	Cement, hydration product, capillary pore	0.5 μm	50 μm × 50 μm × 50 μm (micro-CT structure)
Mortar level	Paste, aggregate and ITZ	0.04 mm	6 mm × 6 mm × 6 mm

Table 5 Mechanical parametersof solid phases in cement-based materials at different scales.

Material scale	Solid phase	Young's modulus (GPa)	Shear modulus (GPa)	Poisson's Ratio	References
Globule level	C-S-H solid	130	52.0	0.25	Inverse deduction
C-S-H gels level	Globule	81.5	32.6	0.25	Inverse deduction
Cement paste level	Unhydrated cement	135	51.9	0.3	[30, 33]
	Inner product	29.4	11.9	0.24	
	Outer product	21.7	8.9	0.24	
Mortar level	Sand	62.5	25.8	0.21	[30]
	Paste matrix	11.8	4.8	0.24	Computed at paste level
	ITZ	10.0	4.0	0.25	Calculated by Eq.(4)&(5)

For convenience, we recall the relation between the bulk modulus K, the shear modulus G, the Young's modulus E and the Poisson's Ratio v [30]:

$$E = \frac{9G}{3+G/K} \quad v = \frac{3-2G/K}{6+2G/K}$$

4.2.1 Lattice networks of C-S-H globule and gels

At C-S-H globule level, the contribution phase for carrying loads is considered as C-S-H solid. At C-S-H gel scale, the contribution phase is assumed as globule. The Young's moduli and shear moduli of C-S-H solid and globule are computed by inverse deduction from those of HD and LD gels.

4.2.2 Lattice network of cement paste

At cement paste scale, for the microstructure from HYMOSTRUC3D, the solid phases are considered as cement, inner product and outer product whose mechanical properties are adopted from literature [30, 33]. For the microstructure obtained by micro-CT, the solid phases are cement and hydration product. The mechanical property of hydration product is adopted to be the weighted average of HD and LD gels.

4.2.3 Lattice network of mortar

At mortar level, the mechanical parameters input are related to sand, paste matrix and ITZ. The mechanical parameters of sand are adopted from literature [30], while those of paste matrix are computed though a uniaxial tension test on the microstructure of cement paste by 3D lattice analysis. The Young's and shear moduli of ITZ are calculated by averaging the corresponding parameters of

sand and paste matrix according to equation (4) and (5). The ITZ thickness equals to the length of a single lattice element.

From the corresponding structures of cement-based materials at different scales described in chapter 3, combining the mechanical parameters of materials concerned at each scale, the lattice networks of cement-based materials at the respective scale have been constructed.

4.3 Imposing internal loads

As RH decreases, the capillary pressure and disjoining pressure give rises. According to Kelvin equation (equation (1)), changes of capillary pressure and disjoining pressure can be calculated.Assuming the atmospheric pressure p_{atm} equals to 0, thenegative liquid pressure p_L can be obtained. It is the determining factor for the drying deformation of cement-based materials through interlayer water, gel water and capillary water. The problem to be solved in this part is how to impose theliquid pressure on the lattice network of cement-based materials at the respective scale. Figure 14 illustratesthe solution.

4.3.1 Loads on C-S-H globule

The action of interlayer water, assumed to be randomly distributed in C-S-H solids, is imposed by applying the negative liquid pressure p_L on the solid walls contacting with interlayer water, as

illustrated in figure 14.The force applied on a C-S-H solid cell, $\mathbf{f}_{nod}$, isan integration of liquid pressure p_L on its associated surfaces $A_L$which is in contact with the contribution water,

$$\mathbf{f}_{nod} = \int_{A_L} p_L \partial A_L \tag{7}$$

4.3.2Loads on C-S-H gels

Similarly, the action of gel water can be imposed on the lattice networks of HD and LD gels respectively. Since gel pores can get empty within 85%-to-50% RH range, air phase in LDgel is assumed to be no contribution to the drying deformation. The drying deformation of globules computed at the last scale is incorporated through applying equivalent stress $\sigma_G$on the globule cells,

$$\sigma_G = E_G \varepsilon_G \tag{8}$$

whereE_G represents the Young's modulus of globule, ε_G represents the linear strain of globule, which is computed at the globule level. Equivalent stress σ_G is defined as the stress applied on the surfaces of one globule cell which will cause the same amount shrinkage of globule cell as interlayer water does at the globule level. By multiplying equivalent stress σ_G by the area of globule cellA_G, equivalent loads representing the drying deformation of globules can be obtained and further are applied on the lattice networks of HD and LD gels.

4.3.3Loads on cement paste

At cement paste scale, the factors responsible for the drying deformation of cement paste are capillary water, shrinkages of HD and LD gels.The negative liquid pressure in capillary pores is active at high RH (≥85% RH), while does not work when the capillary pores get empty below about 85% RH. Similar to the approach considering the contribution of gel water, using equation (7), action of liquid pressure p_{L} is applied on the pore walls those are in contact with capillary water. With regard to inner and outer products, equivalent stress σ_{csh} is introduced, and defined as the stress applied on the surfaces of one inner or outer product cell, which will cause the same amount shrinkage of HDgel or of LDgel as gel water does. The force applied on a solid cell in general can be written asthe resultant force of local liquid pressure action (an integration of liquid pressure p_{L} on its associated surfaces A_{L} where in contact with capillary water) and local shrinkage action of C-S-H gels,

$$\mathbf{f}_{\mathrm{nod}} = \sigma_{\mathrm{csh}} A_{\mathrm{csh}} + \int_{A_{\mathrm{L}}} p_{\mathrm{L}} \partial A_{\mathrm{L}} \qquad (9)$$

For inner product cell, the effective load comes from the equivalent stress on HD gel. For outer product cell, in addition to the equivalent stress on LD gel, the contribution of capillary water can not be neglected at high RH. For cement cell, no effective load is applied. See the illustration in figure 14.

4.3.4Loads on mortar/concrete

At mortar or concrete level, the only factor attributed to its drying shrinkage is the drying deformation of paste matrix. For paste matrix cell, equivalent stress $\sigma_{\mathrm{p}}$is incorporated and equals to,

$$\boldsymbol{\sigma}_p = E_p \boldsymbol{\varepsilon}_p \quad (10)$$

where E_p represents the Young's modulus of paste matrix phase, $\varepsilon_p$represents the linear strain of cement paste, which is computed at cement paste level.Similar to the approach applying equivalent load on globule cells at C-S-H gel level and applying equivalent load on C-S-H gel cell at cement paste level, equivalent load representing the drying deformation of paste matrix can be obtained by multiplying equivalent stress σ_p by the area of paste matrix cell A_p and further are applied on the lattice networks of mortar or concrete.

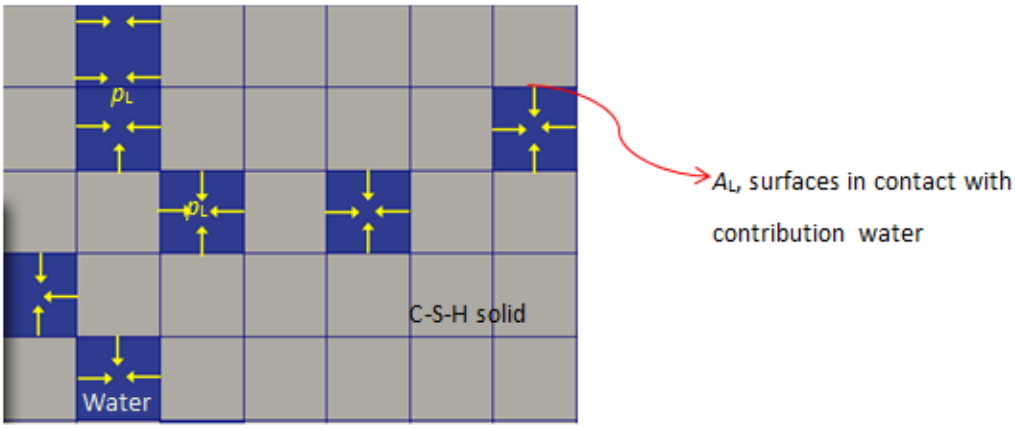

At globule level: contribution of interlayer water.

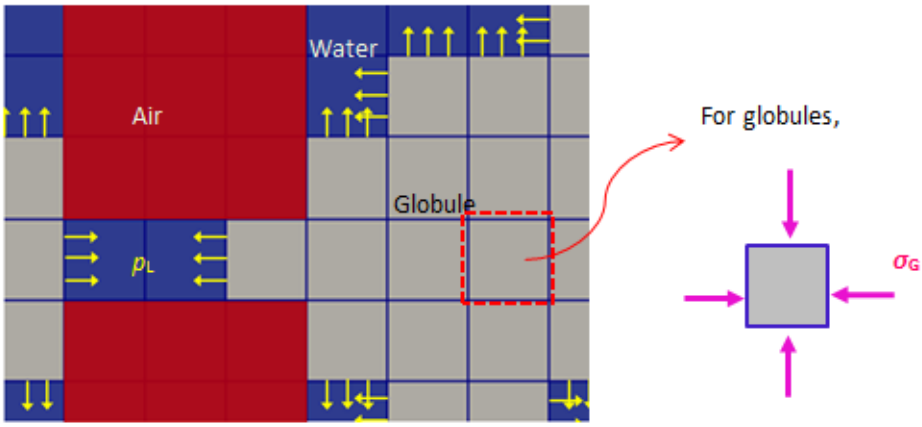

At C-S-H gels level: contribution of gel water and globules whose deformation were computed at globule level.

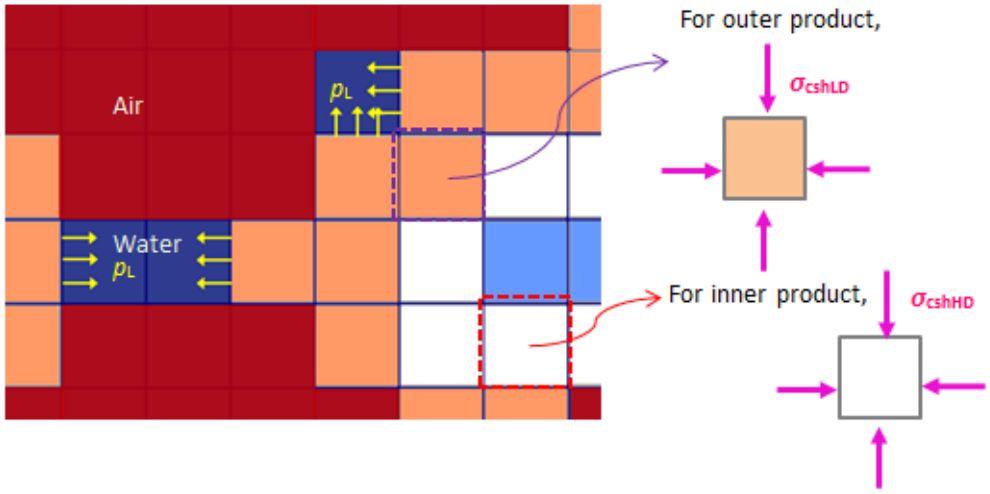

At cement paste level: contribution of capillary water and inner and outer products. Deformations of inner and outer products were obtained at C-S-H gels level.

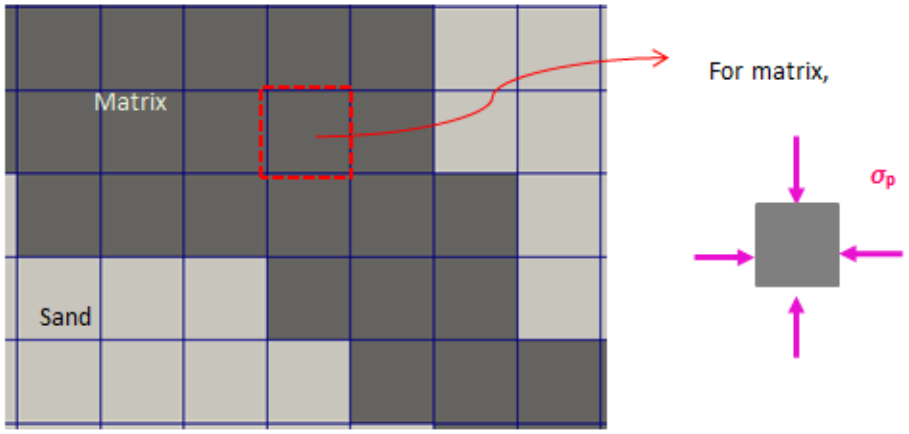

At concrete/mortar level: contribution of paste matrix whose deformation was computed at cement paste level.

Figure 14: Illustration of imposition of internal loads for the multiscale material at each scale.

4.4Computation of stress and strain distribution

Set free boundary condition, the internal stress and strain distribution within each lattice element can be obtained at each specific scale after a kernel computation [33]. From the movements of cells on boundaries, the deformation of the sample can be obtained.

5. Results and discussion

5.1 Drying deformations of C-S-H globule and gels

For C-S-H globule at level 0 and HD gel at level 1, their linear drying deformations are directly proportional to the liquid pressure p_L, see figure 15. Slopes of 5.2 and 26.0 are observed respectively for globule and HD gel. As to LD gel, the slope is steep when p_L ranges from -12MPa to -58MPa (91%-to-65% RH) and gets gentle after -58MPa until -72 MPa (65%-to-59% RH). A deformation decrease of LD gel is observed when p_L= -96 MPa (50% RH). Different from C-S-H globule and HD gel remaining full of water, gel pores in LD C-S-H get empty within 85%-to-50% RH range. Due to the increase of empty gel pores and the decrease of gel water, the dependence of the drying deformation of LD gel on the liquid pressuregets moderate. In addition, figure 15 shows a distinct difference between the upper and the lower values at the same p_L for LD gel. It indicates the statistical fluctuation of LD gel nanostructures generated previously. The effect of statistical fluctuation will be discussed in section 5.4.

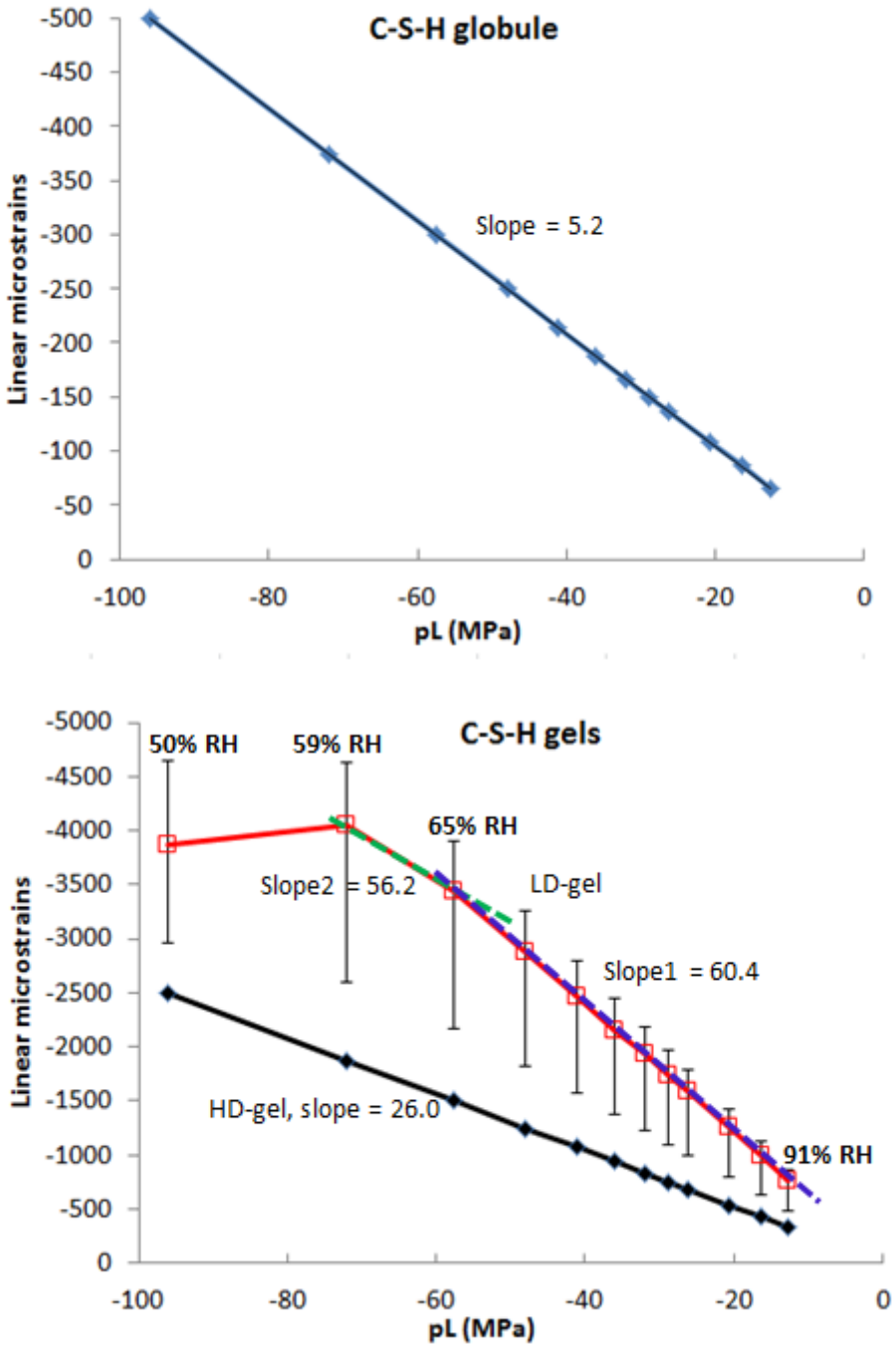

Figure 15: Dependence of linear drying deformation of C-S-H globule and C-S-H gels on liquid pressure p_L.

5.2 Drying deformation and moisture loss of cement paste

Predictions of the drying deformation of cement paste with *w/c* 0.5 after hydrating 28 days are given in figure 16. For comparison, experimental results for ordinary Portland cement pastes with 0.5*w/c* are also plotted.Specification about these paste specimensby experiments are summarized in table 6. In the authors' experiment, specimens were cast in sealed 25 mm diameter plastic vials and shaped into cylinders. After mixing 24 hours, they were demolded and immersed in saturated lime water at about 20 ºC. Before drying, the cylindrical hardened paste was cut into thin discs of 0.8 mm thick and 25 mm in diameter. The paste discs were dried in a desiccator where RH is constant. Their linear drying shrinkage was determined in reference to the saturated status before drying. By using the thin disc specimens, the ultimate shrinkage can be achieved in 6 hours after put into the desiccator. Comparing to the experiments by other researchers[1-2], the testing time is reduced drastically and the hydration effect during the drying period can be prevented. In addition, the tested shrinkage can be assumed as the real free shrinkage of specimens where the internal relative humidity of specimens equals to the environmental relative humidity andthe humidity gradients can be neglected.

As plotted in figure 16, both simulations on the micro-CT structure and on the HYMOSTRUC3D structure show the same trend as experiments do, i.e., an increase of drying shrinkage deformation with the decreasing RH. For the micro-CT structure, at each RH condition, 8 simulations were carried out on samples of 50 μm × 50 μm × 50 μm which were cut from a bigger structure of 100 μm × 100μm × 100 μm. The averaged, upper and lower data were plotted in the curve. Simulations on the micro-CT structure are consistent with the experimental results, but show a large scatter among simulations, especially at low RH. Simulations on the HYMOSTRUC3D structure are slightly lower

than others. This might attributed to the coarser pore structure by simulation, as plotted in figure 9, which led to a larger moisture loss, shown in figure 17.Because of computational limitations, the minimum diameter of cement particles in the HYMOSTRUC3D model is assumed to be 1 μm, while real cements have a certain number of particles with sizes smaller than 1 μm. Additionally, HYMOSTRUC3D models hydration as the expansion of concentric shell around the original cement particles, and does not include precipitation of products such as calcium hydroxide within the pore spaces between particles [23-24]. It should be noted thatthe proposed model in this study can be used combining with an updated version of HYMOSTRUC3D,and can be extend to get the related results by using other hydration models such as uic andCEMHYD3D.

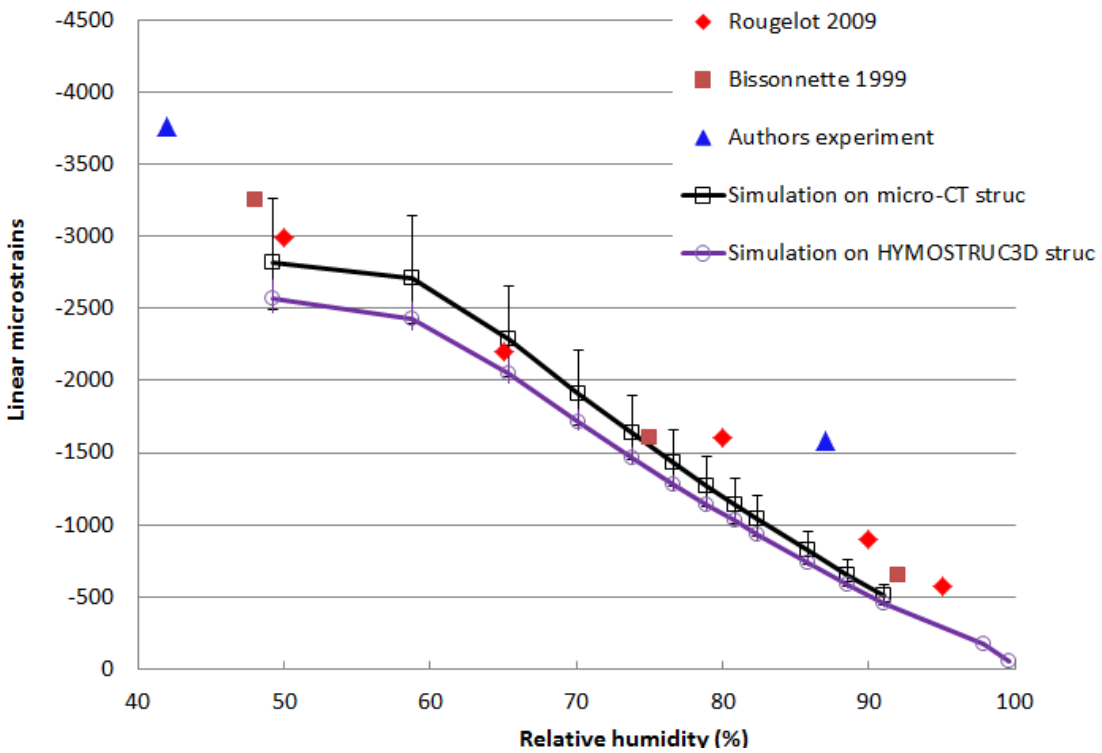

Figure 16: Drying deformation of cement paste (w/c=0.25, 28 days) by simulation and by experiments [1-2].

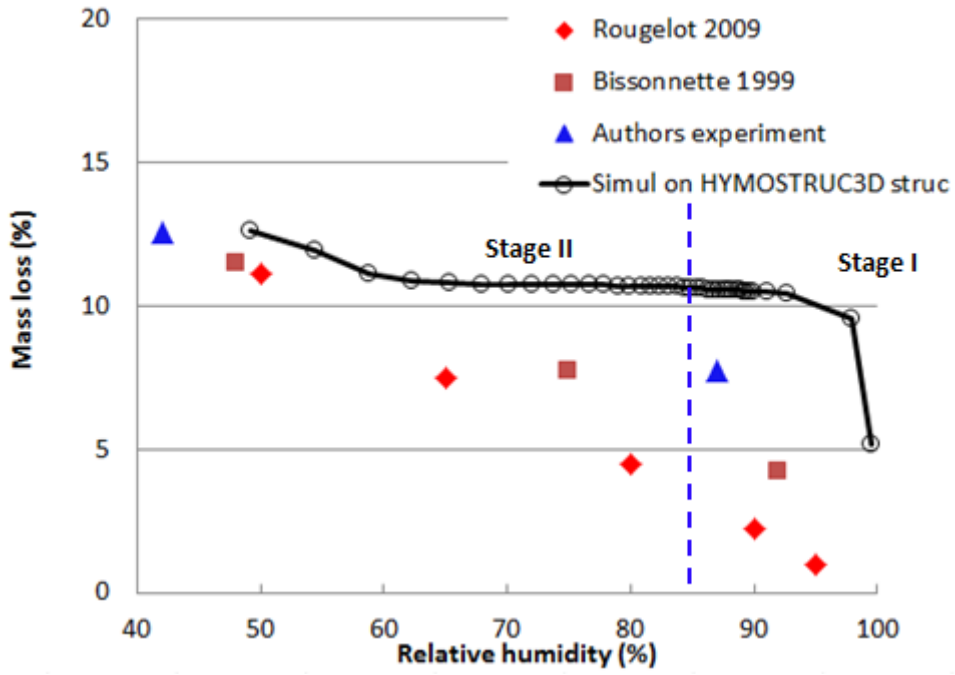

Figure 17: Weight loss of water in cement paste as RH decreases.

Table 6 Specification of cement paste samples (*w/c* 0.5) tested for drying.

Specimen shape and size	Test direction for shrinkage	Curing condition	Ages prior to testing	Time to ultimate shrinkage	References
Prisms of 4*8*32 mm	Length	Lime-saturated water at 23 ºC	28 days	14 days	[1]
Prisms of 20*20*160 mm	Length	Lime-saturated water at 20 ºC	5 months	2 months	[2]
Discs of 0.8 mm thick and 25 mm in diameter	Diameter	Lime-saturated water at 20 ºC	28 days	6 hours	The authors

5.3Drying deformation of mortar

Predictions of the drying deformation of mortar (V_{agg}=0.46; D_{max}=2.0 mm; D_{min}=0.2 mm) are given in figure 18. Predictions are generally in agreement with experiments with the same sand volume fraction, the same *w/c* and the same hydration age.

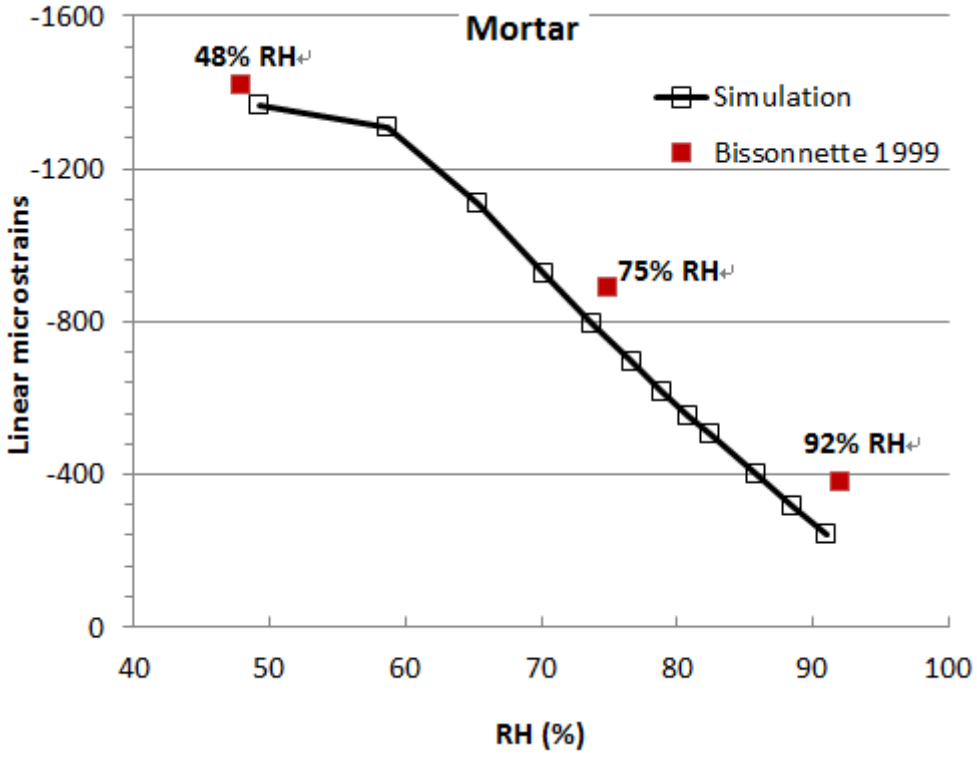

Figure 18: Drying deformation of mortar (V_{agg}=0.46; D_{max}=2.0 mm; D_{min}=0.2 mm) by simulation and by experiment [1].

5.4Discussion about parameter determination and passing-through

Three sources of error: statistical fluctuation, finite size effect and digital resolution [58], may be built in the multiscale digital model which is an approximation of reality. Statistical fluctuation errors come about simplybecause the structure under consideration is random, i.e., the nanostructure of LD-gel, the microstructure of cement paste, the mesostructureof mortar, etc., and can only represent apiece of the material. The effect of statistical fluctuation on the drying deformations of LD-gel at nanoscale level and of cement paste at microscale is obvious, as mentioned in figure 15 and figure 16, while is not significant for mortar, see figure 18.In this study, in order to minimize the effect of statistical fluctuation, simulations on a number of structures of material under consideration, i.e., duplicate simulations on 5 LD-gel structures, on 8 cement paste microstructures by micro-CT and on 3 cement paste microstructures by HYMOSTRUC3D,were carried out and the average, lower and upper values were plotted in figure 15 and figure 16.

Finite size error comes about if thepiece of the material is not big enough to be ‘‘typical’’ of arepresentative size sample,that is, not as largeas the real material [58]. Arepresentative volume element (RVE)is used inthe composite material field to minimize the effect of the finite size. There are various definitions about RVE, see review in [59]. From an experimentalist point of view, it may be argued that the RVE is defined when the scatter in experiments drops to a minimum value [57]. In this case, from the point of view of simulation, the RVE can be considered to be achieved when an increase in its size does not lead to considerable differencesin the investigated properties.The determination of RVE may be related to (i) the maximum size of characteristic phase i.e., the size of the largest particle; and (ii) the modeling methods to obtain the investigated property. It is suggested

that the specimen size should be roughly 2~3 times larger than the largest particle[34, 60-61]. In this study, this criterion was satisfied with at each scale.In addition, in determining the size of RVEat nanoscale for LD-gel and at microscale for cement paste by HYMOSTRUC3D model, as mentioned in section 3.1 and 3.2, the size distribution of characteristic pores (i.e., gel pores and capillary pores) is concerned.And finally, a sample size of 150 nm with the largest globule of 5 nm for LD-gel, and a sample size of 100 μm with the largest cement of 37μm for cement paste were determined. In determining the size of mortar RVE, the sand size distributions with different sample sizes ranging from 5 mm to 10 mm were discussed, and a sample size of 6 mm was determined, which is three times of the size of the largest sand.

Digital resolution could be an import source of error for digital models where the phases of the material are identified by pixels in 2D case and by voxels in 3D case.For finite element or finite difference computations, the “right” resolution is as fine as possible [58].However, huge computational cost would be spent if we over pursuit the small resolution. The obvious solution for finite element discretization is to utilize a compatible mesh. It is suggested that the mesh size should be smaller than the smallest particle. In our case,in addition to the size of the smallest particle, the size of water desorption pores at different scales should be concerned. As listed in table 7, the mesh size is smaller than the size of the smallest particle and the size of water desorption pores for most cases, except for cement paste. Below 85% RH, it can be acceptable to use the mesh size of 1 μm, which is larger than the size of water desorption pores, because only a small amount of liquid water exists in capillary pores which can be neglected.At above 85% RH, capillary pores larger than 12 nm

should be captured where water desorption occurs. It is almost impossible for digital models. This problem is solved via constructing a distributed network of pore voxels by a multi-step digitalization algorithm [16].Voxels of mixed phase composed of outer product and capillary pore are introduced to incorporate the capillary pores ranging from 12nm to 1μm.

Table 7Summary of parameters associated with determining mesh size at different scales.

	Mesh size	Size of the smallest particle	Size of water desorption pores		Corresponding RH (%)
Mortar	0.04 mm	0.2 mm			
Cement paste	1 μm	1 μm	≥ 12 nm (8 nm ~ 10 μm)*		100-to-85
LD-gel	1 nm	5 nm	3~12 nm	(2~8nm)*	85-to-50
HD-gel	1 nm	5 nm	1~3 nm		50-to-25
C-S-H globule	0.1 nm	2.2 nm	≤ 2 nm*		25-to-0

* The size division of water desorption pores at each corresponding RH range were updated in literature [11].

In multiscale modeling, another important problem is the passing-through of parameters during upscaling (nano-to-macro transition) or downscaling (macro-to-nano transition). In this study, a RVE-based parameter-passing scheme was employed to determine the mechanical parameters of solid phases in cement-based materials at different scales, listed in table 5. At cement paste level, the

mechanical parameters of unhydrated cement, inner and outer products were determined by nano-indentation test [30,33]. From the cement paste level, downscaling was performed until to the globule level and upscaling was performed until to the mortar level, to obtain the corresponding parameters of solid phases under concern.Based on the mechanical parameters of inner and outer products, by performing a uniaxial tension test on the nanostructures of HD and LD gels using 3D lattice model, the corresponding parameters of globule at C-S-H gels level were determined by inverse deduction.Continue downscaling in a similar way,, the mechanical parameters of C-S-H solid can also be determinedby inverse deduction. If we perform a uniaxial tension test on the microstructure of cement paste via 3D lattice model, the mechanical parameters of paste matrix in mortar can be obtained.

6. Conclusion

This paper has proposed a multiscale microstructure-based model to investigate the drying behavior of cement-based materials.By combining the multiscale computer-generated structure of cement-based materials with 3D lattice analyses, the drying shrinkage deformations of C-S-H gels, cement paste and mortar are respectively investigated via gradually upscaling.Based on the multiscale structure of cement-based materials, the water desorption process in capillary pores of cement paste corresponding to 100%-to-85% RH range, and that in gel pores of LD-gel corresponding to 85%-to-50% RH range, are incorporated in the model. Predictions about the drying deformation of cement-based materials at each respective scale (i.e., C-S-H globule, HD and LD gels,

cement paste and mortar) are presented.Experimental data for the shrinkage of mortar and cement pastes from literatureand from this study are utilized to validate the proposed model.Finally, three sources of error:statistical fluctuation, finite size effect and digital resolution regarding to the determination of the material structure at different scales as well as thepassing-through of mechanical parameters are discussed.

Acknowledgement

The financial supports of National Natural Science Foundation of China via Grant No.51308187& No.51461135001 and Natural Science Foundation of Jiangsu Province via Grant No.BK20130837 are greatly acknowledged.The authors would like to thank the researchers at University of Illinois at Urbana-Champaign (UIUC) for providing the X-ray micro-CT test dataof cement paste.

References

[1] Bissonnette, B., Pierre, P., Pigeon, M. Influence of key parameters on drying shrinkage of cementitious materials, Cement and Concrete Research 29 (10)(1999) 1655-1662.

[2] Rougelot, T., Skoczylas, F., Burlion, N., Water desorption and shrinkage in mortars and cement pastes: Experimental study and poromechanical model, Cement and Concrete Research 39(1)(2009) 35-48.

[3] Kawashima, S.,Shah, S.P., Early-age autogenous and drying shrinkage behavior of cellulose fiber-reinforced cementitious materials, Cement and Concrete Composites 33(2)(2011) 201-208.

[4] Idiart, A., Bisschop, J., Caballero, A., Lura, P., A numerical and experimental study of aggregate-induced shrinkage cracking in cementitious composites,Cement and Concrete Research 42(2)(2012) 272-281.

[5] Sant, G., The influence of temperature on autogenous volume changes in cementitious materials containing shrinkage reducing admixtures, Cement and Concrete Composites34(7)(2012) 855-865.

[6] Zhang, J., Gao, Y., Wang, Z.B., Evaluation of shrinkage induced cracking performance of low shrinkage engineered cementitious composites by ring tests, Composites Part B: Engineering 52(2013) 21-29.

[7] Maruyama, I., Nishioka, Y., Igarashi, G., Matsui, K., Microstructural and bulk property changes in hardened cement paste during the first drying process, Cement and Concrete Research58(2014) 20-34.

[8] Wyrzykowski, M., Lura, P., The effect of external load on internal relative humidity in concrete, Cement and Concrete Research 65(2014) 58-63.

[9] Vlahinić, I., Jennings, H.M., Thomas, J.J., A constitutive model for drying of a partially saturated porous material, Mechanics of Materials 41(2009) 319-328.

[10] Wu, Z., Wong, H.S., Buenfeld, N.R., Influence of drying-induced microcracking and related size effects on mass transport properties of concrete, Cement and Concrete Research, 68 (2015) 35-48.

[11] Jennings, H.M., Kumar A., Sant G., Quantitative discrimination of the nano-pore-structure of cement paste during drying: New insights from water sorption isotherms, Cement and Concrete Research 76 (2015) 27-36.

[12] Bentz, D.P., Garboczi, E.J., Quenard, D.A., Modelling drying shrinkage inreconstructedporous materials: application to porous vycor glass, Modelling and Simulation in Materials Science and Engineering 6 (3)(1998) 211–236.

[13] Coussy, O., Dangla, P., Lassabatere, T., Baroghel-Bouny, V., The equivalent pore pressure and the swelling and shrinkage of cement-based materials, Materials and Structures 37(2004) 15-20.

[14] Chen, L., Rougelot, T., Chen, D.,Shao, J.F., Poroplastic damage modeling of unsaturated cement-based materials, Mechanics Research Communications 36(8)(2009) 906-915.

[15] Grasley, Z.C., Leung, C.K., Desiccation shrinkage of cementitious materials as an aging, poroviscoelastic response, Cement and Concrete Research41 (2011) 77-89.

[16] Liu, L., Chen, H.S., Wan, C.J., Shen, D.J., Microstructure-based modelling of the three-dimensional nature of drying of cementitious materials at high humidity, Computer-Aided Civil and Infrastructure Engineering (2015) under review.

[17] Pinson, M.B., Masoero, E., Bonnaud, P.A., Manzano, H., Ji Q., Yip, S., Thomas, J.J., Bazant, M.Z., van Vliet, K.J., Jennings, H.M., Hysteresis from multiscale porosity: modeling water sorption and shrinkage in cement paste, Physical Review Applied 3 (2015) 064009.

[18] Lura, P., Autogenous deformation and internal curing of concrete, PhD thesis, Delft University of Technology, Delft, 2003.

[19] Coussy, O., Mechanics and Physics of Porous Solids, John Wiley & Sons Ltd, 2010.

[20] Grasley, Z.C., Lange, D.A., D'Ambrosia, M.D., Drying stresses and internal relative humidity in concrete, in: J. Skalny (Ed.), Materials Science of Concrete, vii, American Ceramic Society, 2005, pp. 265–305.

[21] Scherer, G.W., Drying, shrinkage, and cracking of cementitious materials, Transport in Porous Media (2015).

[22] Pichler, C., Lackner, R., Mang, H.A., A multiscale micromechanics model for the autogenous-shrinkage deformation of early-age cement-based materials, Engineering Fracture Mechanics 74 (2007) 34-58.

[23] Liu, L., Ye, G., Schlangen, E., Chen, H.S., Qian, Z.W., Sun, W.,van Breugel, K., Modeling of the internal damage of saturated cement paste due to ice crystallization pressure during freezing, Cement and Concrete Composites33(5)(2011) 562-571.

[24] Liu, L., Sun, W.,Ye, G., Chen, H.S., Qian, Z.W., Estimation of the ionic diffusivity of virtual cement paste by random walk algorithm, Construction and Building Materials28(1)(2012)405-413.

[25] Liu, L., Chen, H.S., Sun, W., Ye, G.Microstructure-based modeling of the diffusivity of cement paste with micro-cracks, Construction and Building Materials 38 (2013)1107-1116.

[26] Liu, L., Shen, D.J., Chen, H.S., Sun, W., Qian, Z.W., Zhao, H.T., Jiang, J.H., Analysis of damage development in cement paste due to ice nucleation at different temperatures, Cement and Concrete Composites53 (2014) 1-9.

[27] Liu, L, Wu, S.X., Chen, H.S., Zhao, H.T., Numerical investigation of the effects of freezing on micro-internal damage and macro-mechanical properties of cement pastes, Cold Regions Science and Technology106~107(2014) 141-152.

[28] Liu, L., Shen, D.J., Chen, H.S., Xu, W.X., Aggregate shape effect on the diffusivity of mortar: A 3D numerical investigation by random packing models of ellipsoidal particles and of convex polyhedral particles, Computers and Structures 144(2014)40-51.

[29] Bernard O., Ulm F-J., Lemarchand E., A multiscale micromechanics-hydration model for the early-age elastic properties of cement-based materials, Cement and Concrete Research 33 (2003) 1293-1309.

[30] Ulm, F.-J., Constantinides, G., Heukamp, F.H. Is concrete a poromechanics material? - A multiscale investigation of poroelastic properties, Materials and Structures37(2004) 43-58.

[31] Nguyen, V.P., Multiscale failure modelling of quasi-brittle materials, PhD thesis, Delft University of Technology, Delft, 2011.

[32] Nguyen, V.P., Stroeven, M., Sluys, L.J., Multiscale failure modeling of concrete: micromechanical modeling, discontinuous homogenization and parallel computations, Computer Methods in Applied Mechanics and Engineering 201-204 (2012) 139-156.

[33] Qian, Z.W., Multiscale modeling of fracture process in cementitious materials, PhD thesis, Delft University of Technology, Delft, 2012.

[34] Zhang, M.Z., Multiscale Lattice Boltzmann-Finite Element Modeling of Transport Properties in Cement-based Materials, PhD thesis, Delft University of Technology, Delft, 2013.

[35] Jennings, H.M., Refinements to colloid model of C-S-H in cement: CM-II, Cement and Concrete Research38(2008) 275-289.

[36] Lide, D.R., CRC Handbook of Chemistry and Physics, CRC Press,2001.

[37] Papatzani S., Paine K., Calabria-Holley J., A comprehensive review of the models on the nanostructure of calcium silicate hydrates, Construction and Building Materials 74 (2015) 219-234.

[38] Jennings, H.M., Thomas, J.J., Gevrennov, J.S., Constantinides, G., Ulm, F-J. A multi-technique investigation of the nanoporosity of cement paste, Cement and Concrete Research 37(2007) 329-336.

[39] Thomas, J.J., Jennings, H.M., A colloidal interpretation of chemical aging of the C-S-H gel and its effects on the properties of cement paste, Cement and Concrete Research36(2006) 30-38.

[40] Jennings, H.M. A model for the microstructure of calcium silicate hydrate in cement paste, Cement and Concrete Research 30 (2000) 101-116.

[41] Fonseca, P.C., Jennings, H.M., The effect of drying on early-age morphology of C-S-H as observed in environmental SEM, Cement and Concrete Research 40 (2010) 1673-1680.

[42] Allen, A.J., Thomas, J.J. & Jennings, H.M., Composition and density of nanoscale calcium-silicate-hydrate in cement, Nature Materials 6(2007) 311-316.

[43] Fonseca, P.C., Jennings, H.M., Andrade, J.E., A nanoscale numerical model of calcium silicate hydrate, Mechanics of Materials 43(2011) 408-409.

[44] Ma H., Hou D., Lu Y., Li Z., Two-scale modeling of the capillary network in hydrated cement paste, Construction and Building Materials 64 (2014) 11-21.

[45] Zhang, M.Z., He Y., Ye, G., Lange, D.A. and van Breugel, K., Computationalinvestigation on mass diffusivity in Portland cement paste based on X-ray computedmicrotomography (μCT) image, Construction and Building Materials27(1) (2012) 472-481.

[46] Garboczi, E.J., Kushch, V.I., Computing elastic moduli on 3-D X-ray computed tomography image stacks, Journal of the Mechanics and Physics of Solids 76(2015) 84-97.

[47] Trtik, P., Münch, B.,Lura, P.,A critical examination of statistical nanoindentation on model materials and hardened cement pastes based on virtual experiments, Cement and Concrete Composites 31(10)(2009) 705-714.

[48] Lura, P., Trtik, P., Münch, B., Validity of recent approaches for statistical nanoindentation of cement pastes,Cement and Concrete Composites 33 (2011) 457-465.

[49] Chen-Wiegart, Y.K., Camino, F.E., Wang, J., Sample preparation of energy materials for X-ray nanotomography with micromanipulation, ChemPhysChem 15 (8)(2014) 1587-1591.

[50] van Breugel, K., Simulation of hydration and formation of structure in hardening cement-based materials, PhD thesis, Delft University of Technology, Delft, 1991.

[51] Ye, G., Experimental study and numerical simulation of the development of the microstructure and permeability of cementitious materials, PhD thesis, Delft University of Technology, Delft, 2003.

[52] Bentz, D.P., Garboczi, E.J., Percolation of phases in a three-dimensional cement paste microstructure model,Cement and Concrete Research 21 (2-3)(1991) 325-344.

[53] Bishnoi, S., Schrivener, K.L., A new platform for modeling the hydration of cements, Cement and Concrete Research 39 (4)(2009) 266-274.

[54] Mindess, S. & Young, J.F., Concrete, Prentice-Hall, Englewood Cliffs, 1981.

[55] Schlangen, E., Experimental and numerical analysis of fracture processes in concrete, PhD thesis, Delft University of Technology, Delft, 1993.

[56] Yip, M., Mohle, J., Bolander, J.E., Automated modeling of three-dimensional structural components using irregular lattices, Computer-Aided Civil and Infrastructure Engineering20 (6) (2005)393-407.

[57] van Mier, J.G.M., Concrete Fracture: a Multiscale Approach, CRC Press, 2012.

[58] Garboczi E.J., Bentz D.P.,The effect of statistical fluctuation, finite sizeerror, and digital resolution on the phase percolation and transportproperties of the NIST cement hydration model, Cement and Concrete Research31(10)(2001)1501-1514.

[59] Gitman I.M., Askes H., Sluys L.J., Representative volume: Existence and size determination, Engineering Fracture Mechanics 74 (16)(2007) 2518–2534.

[60] Chen H.S, Stroeven P., Sluys L.J., Sun W., An approach to determine the size of representative volume element (RVE) for microstructural parameters of cementitious composites. In: Proceedings of the 13th International Congress on the Chemistry of Cement, 2011, Madrid, Spain, paper No.553.

[61] Wu, Q., Rougelot, T., Burlion, N., Bourbon, X., Representative volume element estimation for desorption isotherm of concrete with sliced samples. Cement and Concrete Research 76 (2015) 1-9.

Table 1: A summary of pore empty processes [11] and contribution water to the drying deformation.

Relative humidity (RH, %)	Water desorption process	Contribution water to the drying deformation
100-to-85	Capillary pores empty by a pore blocking mechanism.	Capillary water LD-gel water HD-gel water interlayer water
85-to-50	LD-gel pores empty by pore blocking.	LD-gel water HD-gel water interlayer water
50-to-25	HD-gel pores continue to empty by pore blocking.	HD-gel water interlayer water

Table 2Material parameters utilized in the HYMOSTRUC3D model for cement paste.

Cement type	Portland CEM I 42.5N
Mineralogical composition of cement	64% C_3S, 13% C_2S, 8% C_3A, 9% C_4AF by mass
Fineness (Blaine surface area value) of cement	420 m^2/kg
Minimum diameter of cement particle	1 μm
Maximum diameter of cement particle	50 μm
Size interval of cement particles	1 μm
Water-to-cement ratio	0.5

Table 3 Volume fractions of hydration products of cement paste by HYMOSTRUC3D and by micro-CT (Computed at a resolution of 0.25 μm/voxel for HYMOSTRUC3D and 0.5 μm/voxel for micro-CT).

	Unhydrated cement	Inner product	Outer product	Capillary pore
By HYMOSTRUC3D	0.095	0.289	0.412	0.204
By micro-CT	0.102	0.711		0.187

Table 4 Specification of lattice networks

Material scale	Composition phases	Mesh size	Specimen size
Globule level	C-S-H solid and interlayer water	0.1 nm	5 nm × 5 nm × 5 nm
C-S-H gel level	Globule and gel pore	1 nm	100 nm × 100 nm × 100 nm (HD gel) 150 nm × 150 nm × 150 nm (LDgel)
Cement paste level	Cement, inner product, outer product and capillary pore	1 μm	100 μm × 100 μm × 100 μm (HYMOSTRUC3D structure)
	Cement, hydration product, capillary pore	0.5 μm	50 μm × 50 μm × 50 μm (micro-CT structure)
Mortar level	Paste, aggregate and ITZ	0.04 mm	6 mm × 6 mm × 6 mm

Table 5 Mechanical parameters of solid phases in cement-based materials at different scales.

Material scale	Solid phase	Young's modulus (GPa)	Shear modulus (GPa)	Poisson's Ratio	References
Globule level	C-S-H solid	130	52.0	0.25	Inverse deduction
C-S-H gels level	Globule	81.5	32.6	0.25	Inverse deduction
Cement paste level	Unhydrated cement	135	51.9	0.3	[30, 33]
	Inner product	29.4	11.9	0.24	
	Outer product	21.7	8.9	0.24	
Mortar level	Sand	62.5	25.8	0.21	[30]
	Paste matrix	11.8	4.8	0.24	Computed at paste level
	ITZ	10.0	4.0	0.25	Calculated by Eq.(4)&(5)

For convenience, we recall the relation between the bulk modulus K, the shear modulus G, the Young's modulus E and the Poisson's Ratio v [30]:

$$E = \frac{9G}{3+G/K} \quad v = \frac{3-2G/K}{6+2G/K}$$

Table 6 Specification of cement paste samples (*w/c* 0.5) tested for drying.

Specimen shape and size	Test direction for shrinkage	Curing condition	Ages prior to testing	Time to ultimate shrinkage	References
Prisms of 4*8*32 mm	Length	Lime-saturated water at 23 ºC	28 days	14 days	[1]
Prisms of 20*20*160 mm	Length	Lime-saturated water at 20 ºC	5 months	2 months	[2]
Discs of 0.8 mm thick and 25 mm in diameter	Diameter	Lime-saturated water at 20 ºC	28 days	6 hours	The authors

Table 7Summary of parameters associated with determining mesh size at different scales.

	Mesh size	Size of the smallest particle	Size of water desorption pores		Corresponding RH (%)
Mortar	0.04 mm	0.2 mm			
Cement paste	1 μm	1 μm	≥ 12 nm (8 nm ~ 10 μm)*		100-to-85
LD-gel	1 nm	5 nm	3~12 nm	(2~8nm)*	85-to-50
HD-gel	1 nm	5 nm	1~3 nm		50-to-25
C-S-H globule	0.1 nm	2.2 nm	≤ 2 nm*		25-to-0

* The size division of water desorption pores at each corresponding RH range were updated in literature [11].

Figure(s)

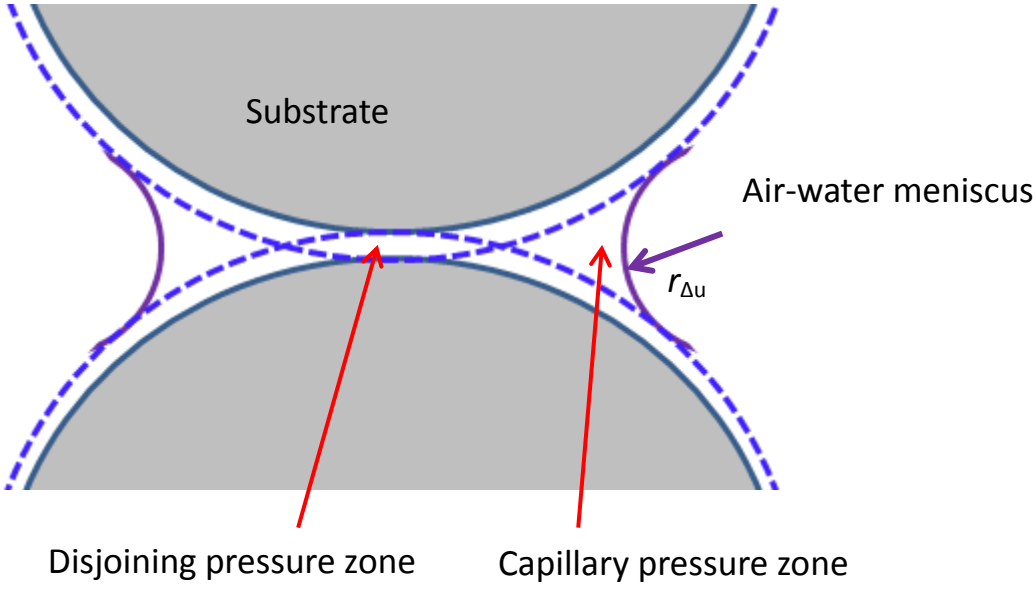

Figure 1: Geometrical illustration of capillary adhesion and disjoining pressure zones.

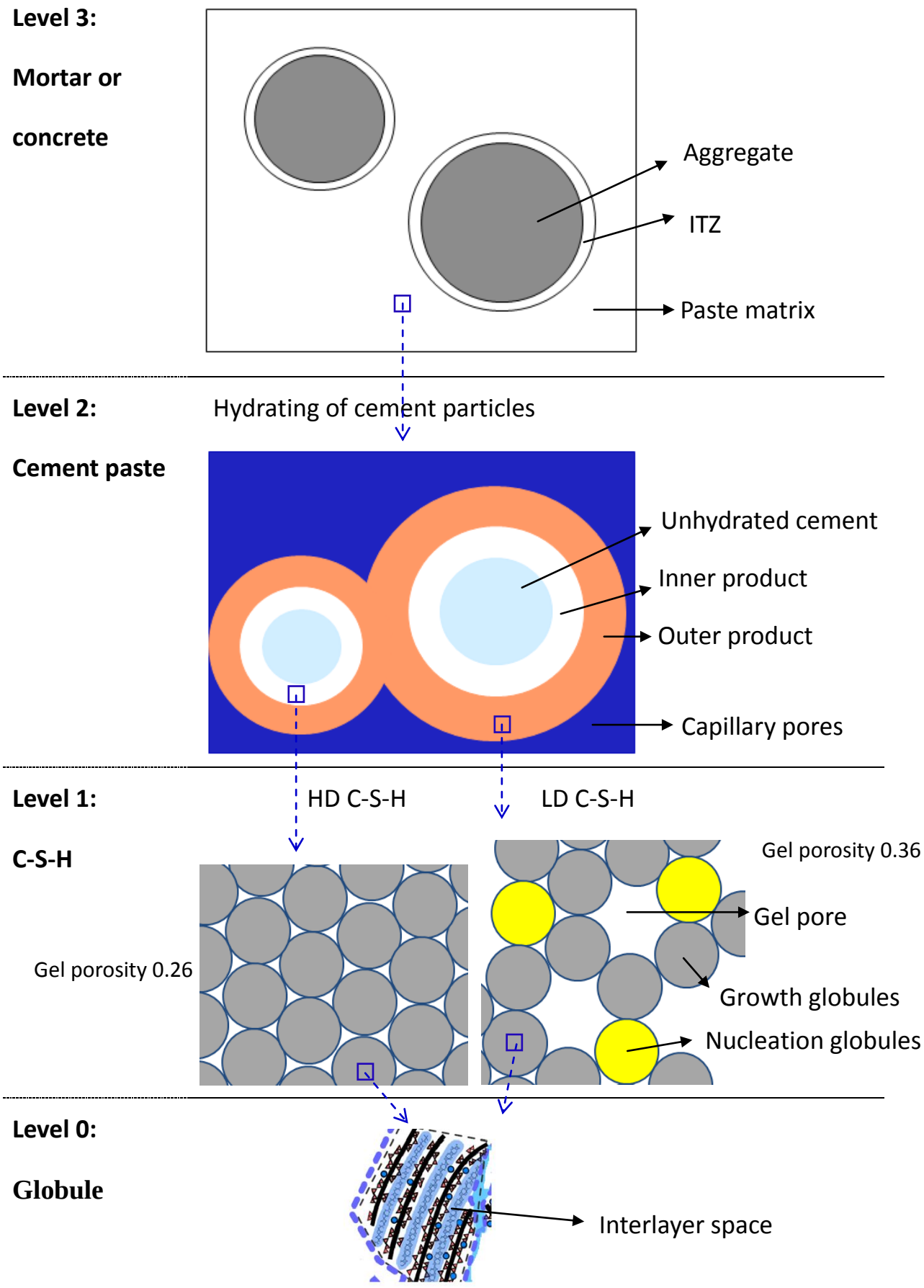

Figure 2: Multiscale structure of cement-based materials [11, 16].

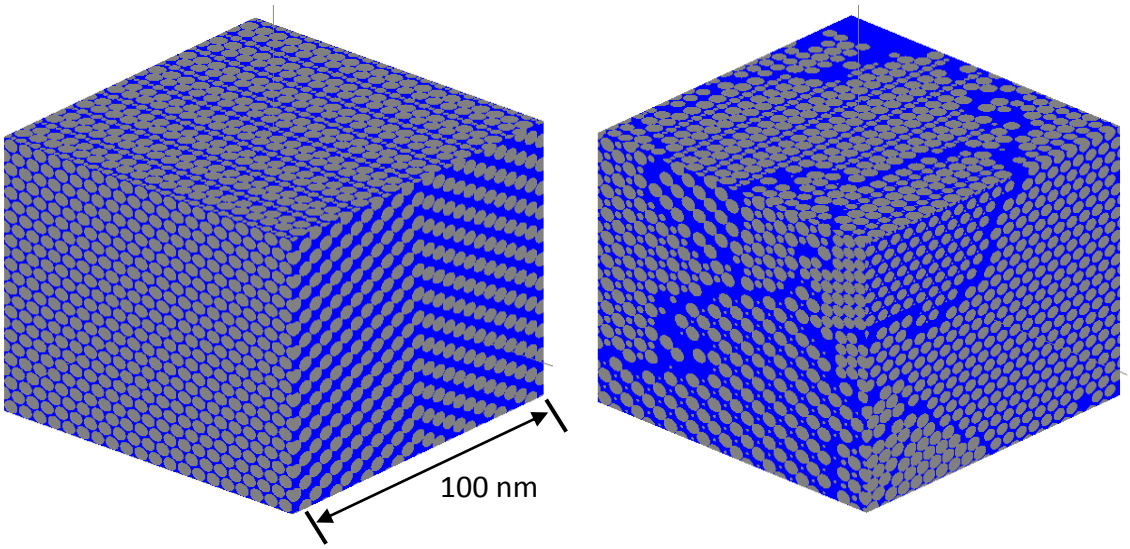

Figure 3: Simulated nanostructures of HD-gel (left) and LD-gel (right).

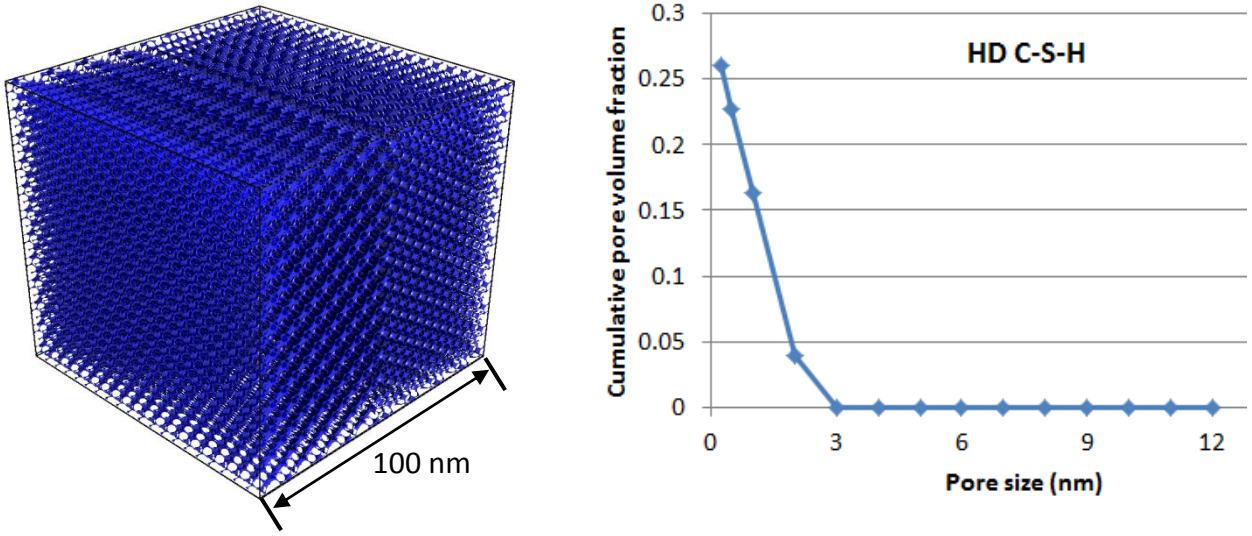

Figure 4: Pore structure (left) and pore size distribution (right) of HD-gel.

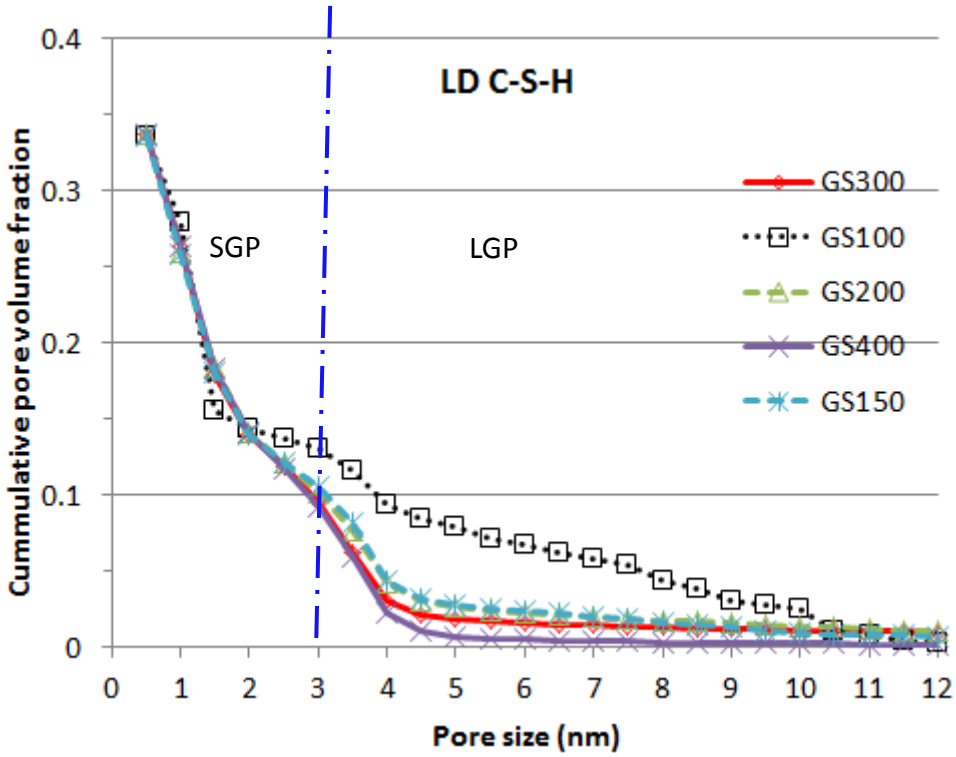

Figure 5: Simulated gel pore size distribution of LD C-S-H with various side lengths.

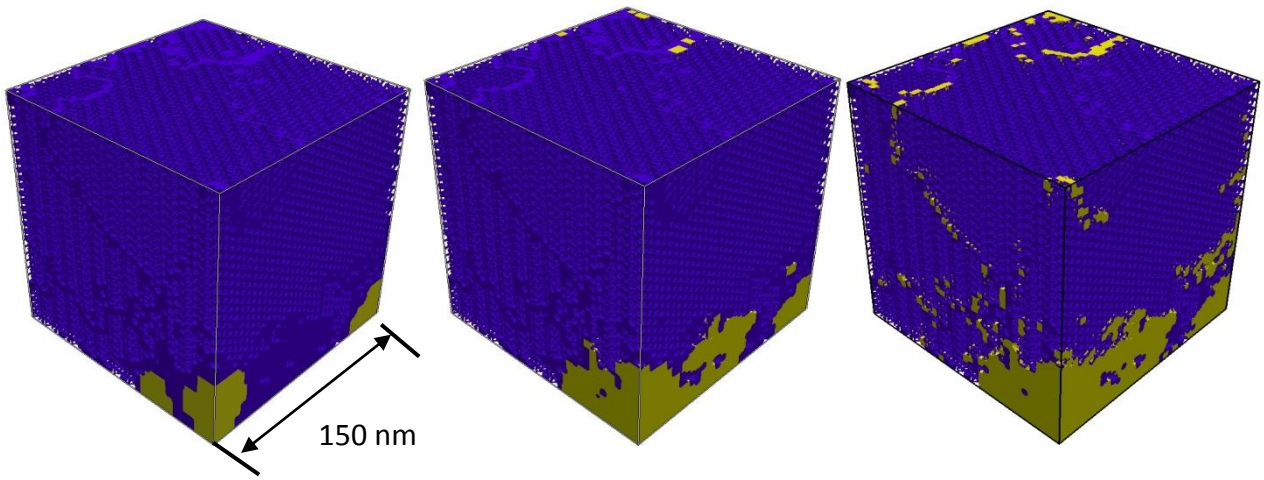

81% RH 65% RH 50% RH

Figure 6: Changes of gas-liquid phase in LD-gel as RH decreases (yellow: air; blue: water) (Displayed at a resolution of 0.5 nm/voxel).

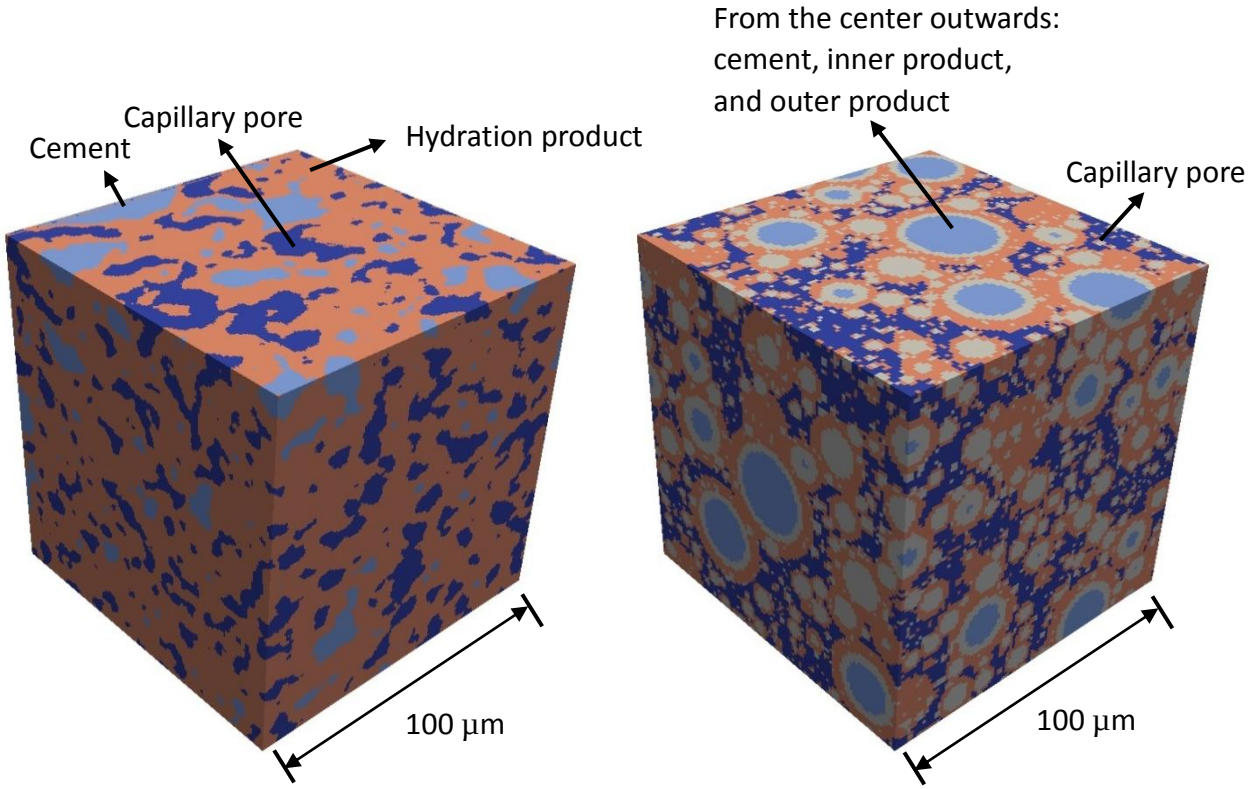

Figure 7: Microstructures of cement paste (CEMI 42.5R, *w/c* 0.5, 28 days). Left: cement paste by Micro-CT; Right: cement paste by HYMOSTRUC3D.

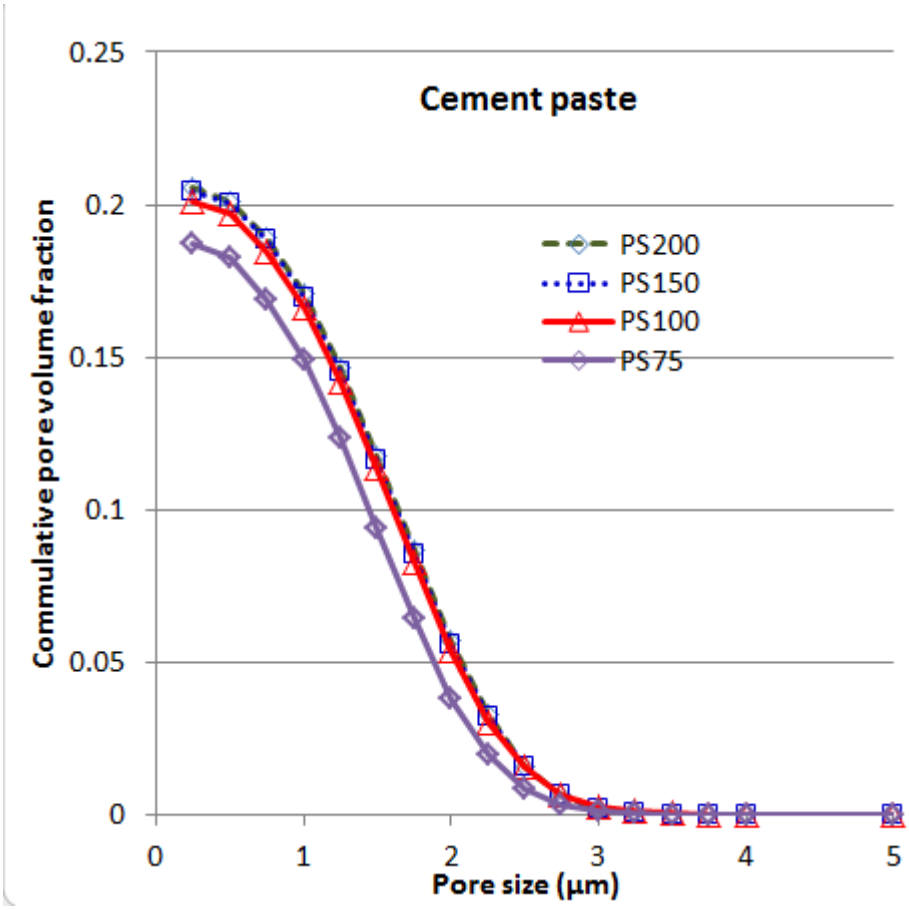

Figure 8: Simulated capillary pore size distribution of cement paste (CEMI 42.5R, *w/c* 0.5, 28 days) from HYMOSTRUC3D.

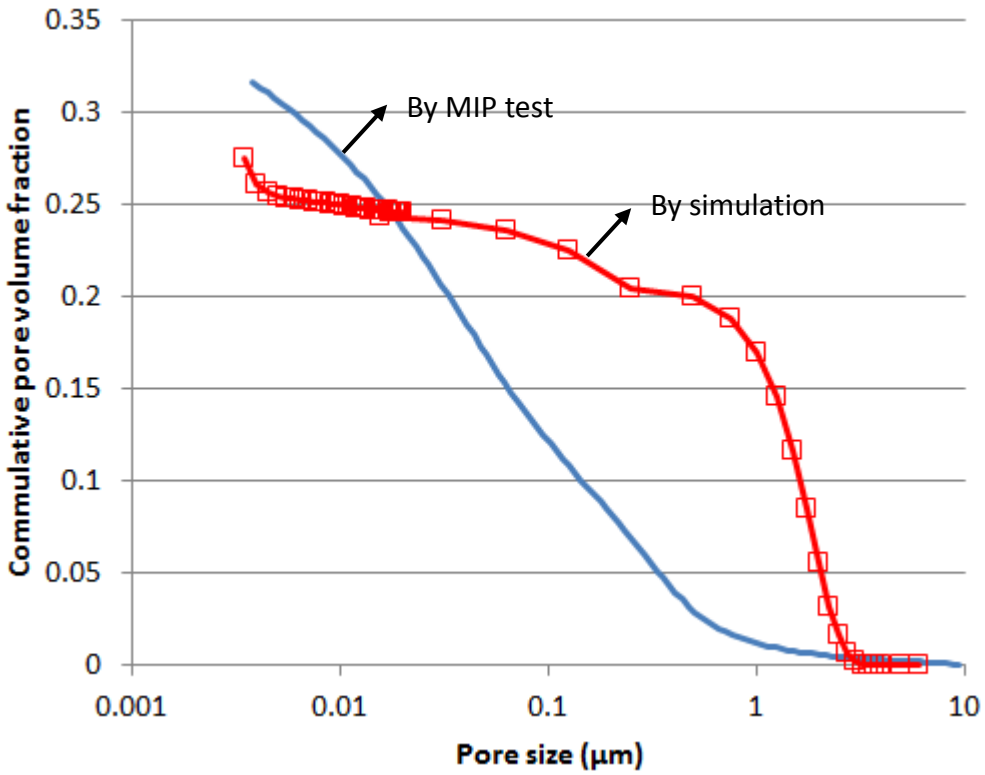

Figure 9: Pore size distribution curves of cement paste (CEMI 42.5R, *w/c* 0.5, 28 days) by simulation and MIP test [51].

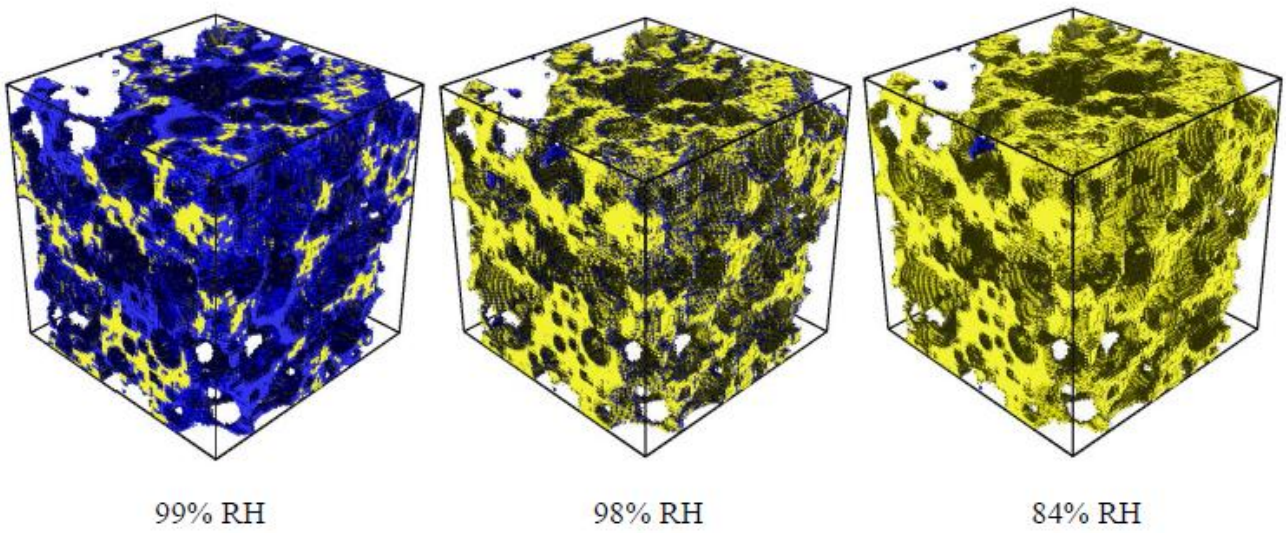

Figure 10: Gas-liquid phase in the pore structure of cement paste under different RH (yellow: air, blue: water. Capillary pores larger than 10 nm are illustrated). [16]

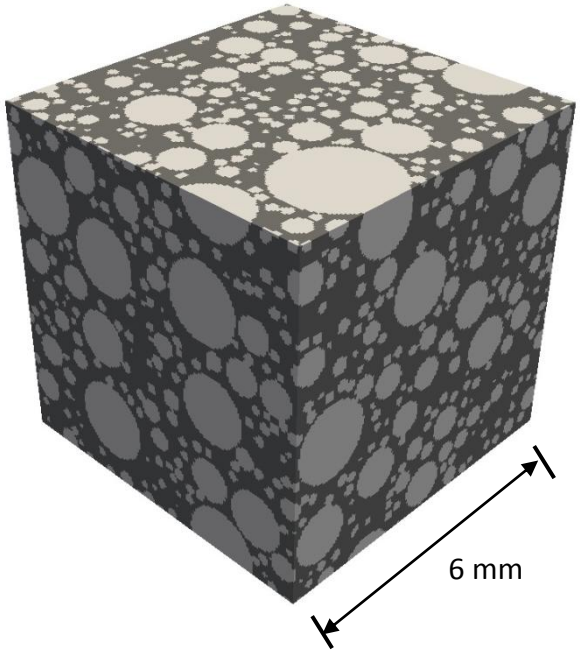

Figure 11: Mesostructure of mortar (Dark: paste matrix; white: sand. V_{agg}=0.46; D_{max}=2.0 mm; D_{min}=0.2 mm).

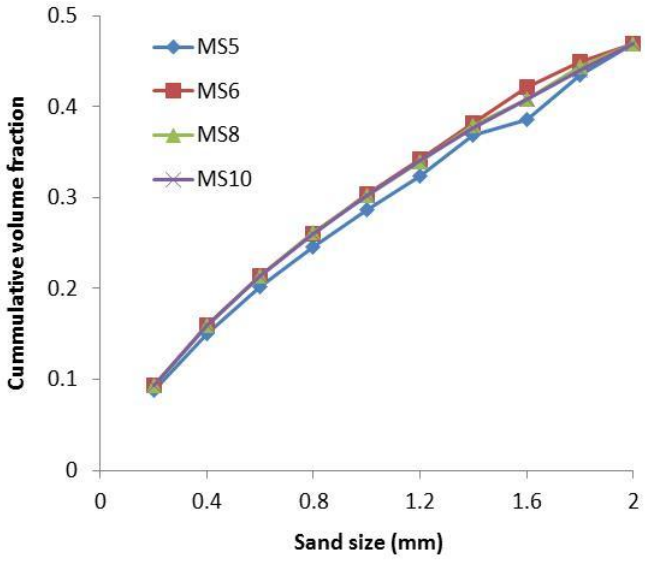

Figure 12: Sand size distributions of mortar (V_{agg}=0.46; D_{max}=2.0 mm; D_{min}=0.2 mm).

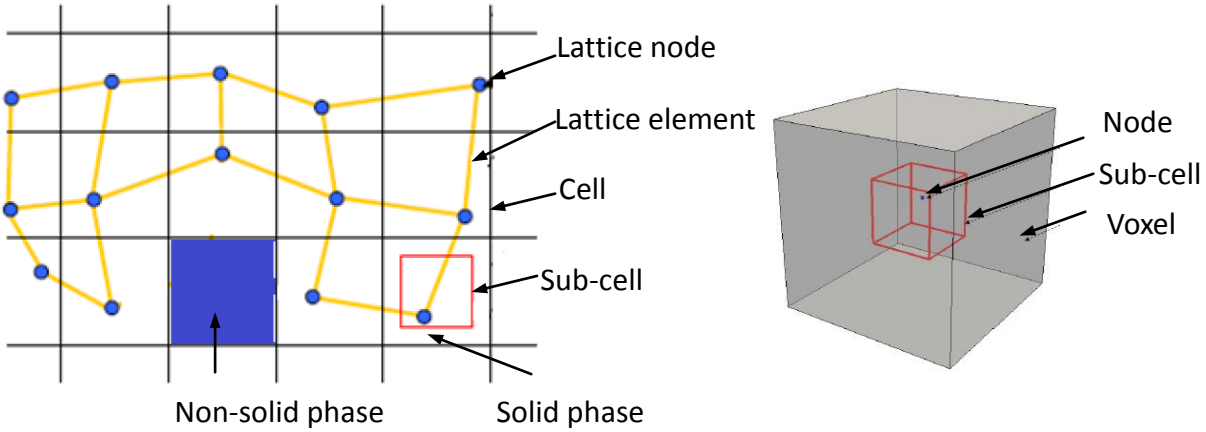

Figure 13: Lattice network construction by a quadrangular approach (reproduced after [33]).

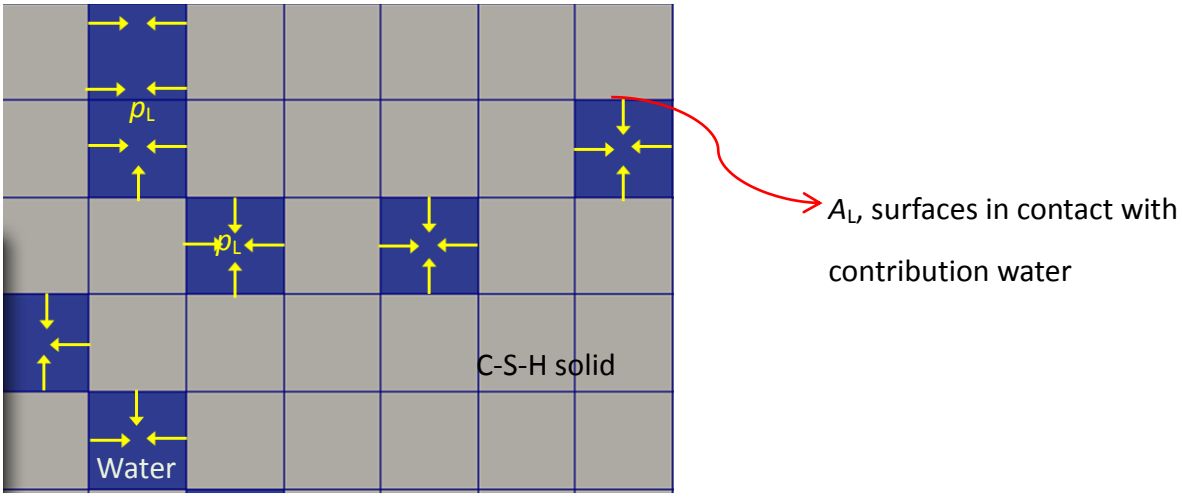

At globule level: contribution of interlayer water.

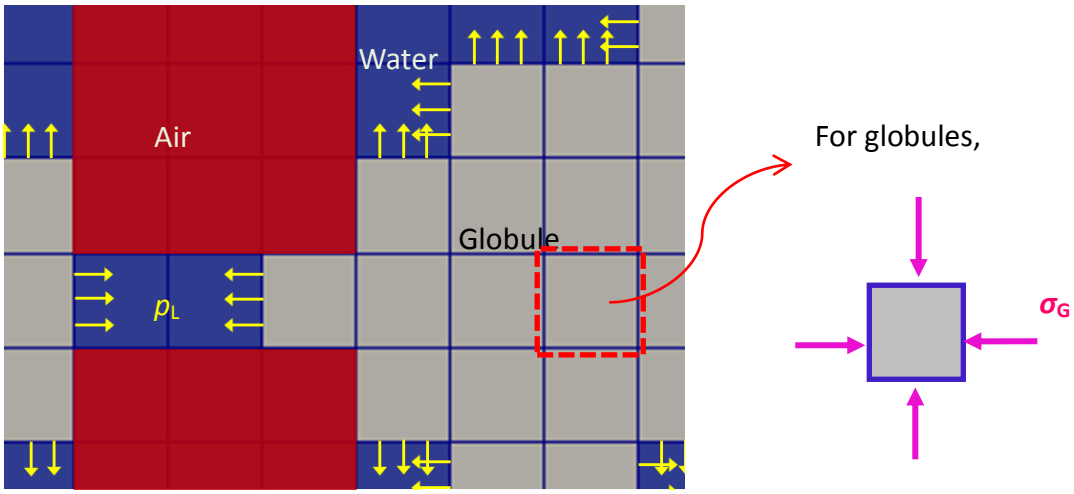

At C-S-H gels level: contribution of gel water and globules whose deformation were computed at globule level.

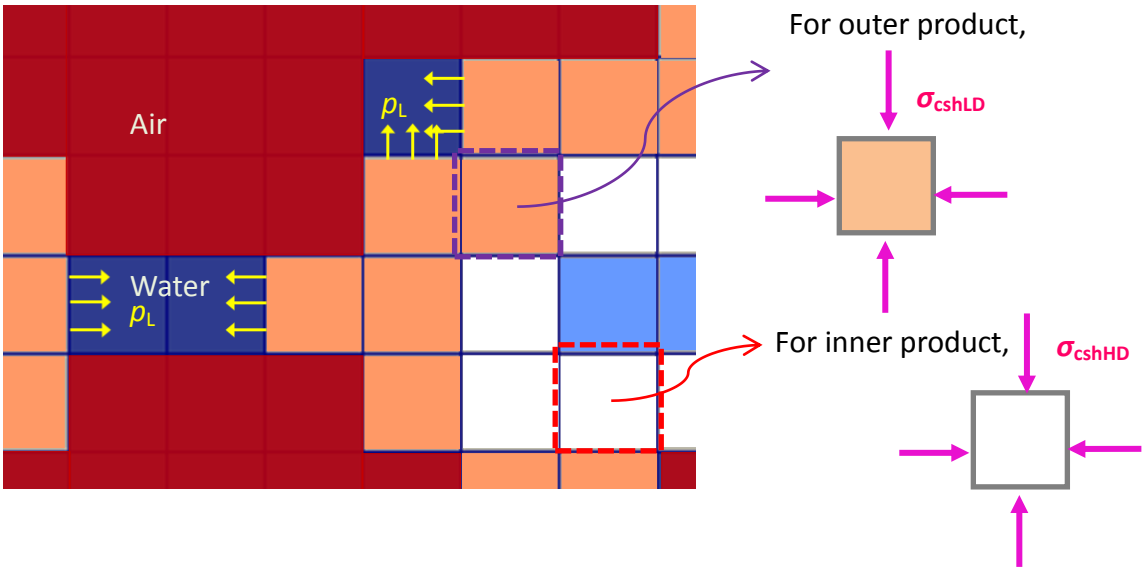

At cement paste level: contribution of capillary water and inner and outer products. Deformations of inner and outer products were obtained at C-S-H gels level.

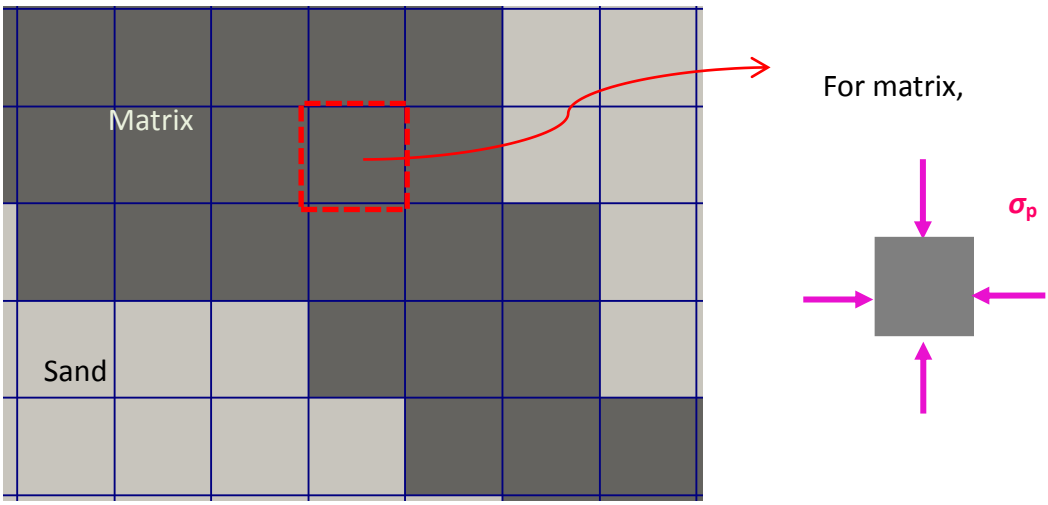

At concrete/mortar level: contribution of paste matrix whose deformation was computed at cement paste level.

Figure 14: Illustration of imposition of internal loads for the multiscale material at each scale.

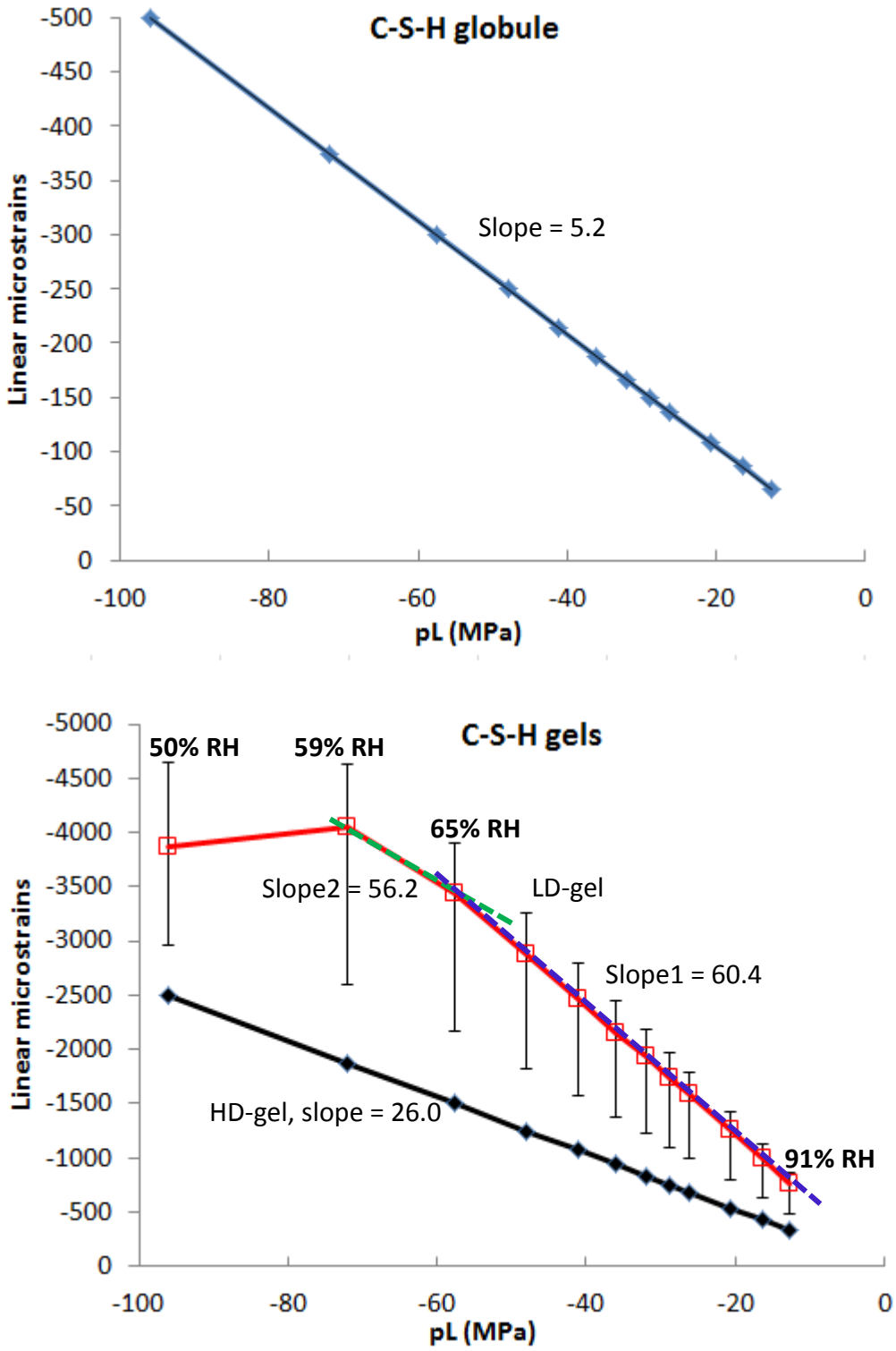

Figure 15: Dependence of linear drying deformation of C-S-H globule and C-S-H gels on liquid pressure p_L.

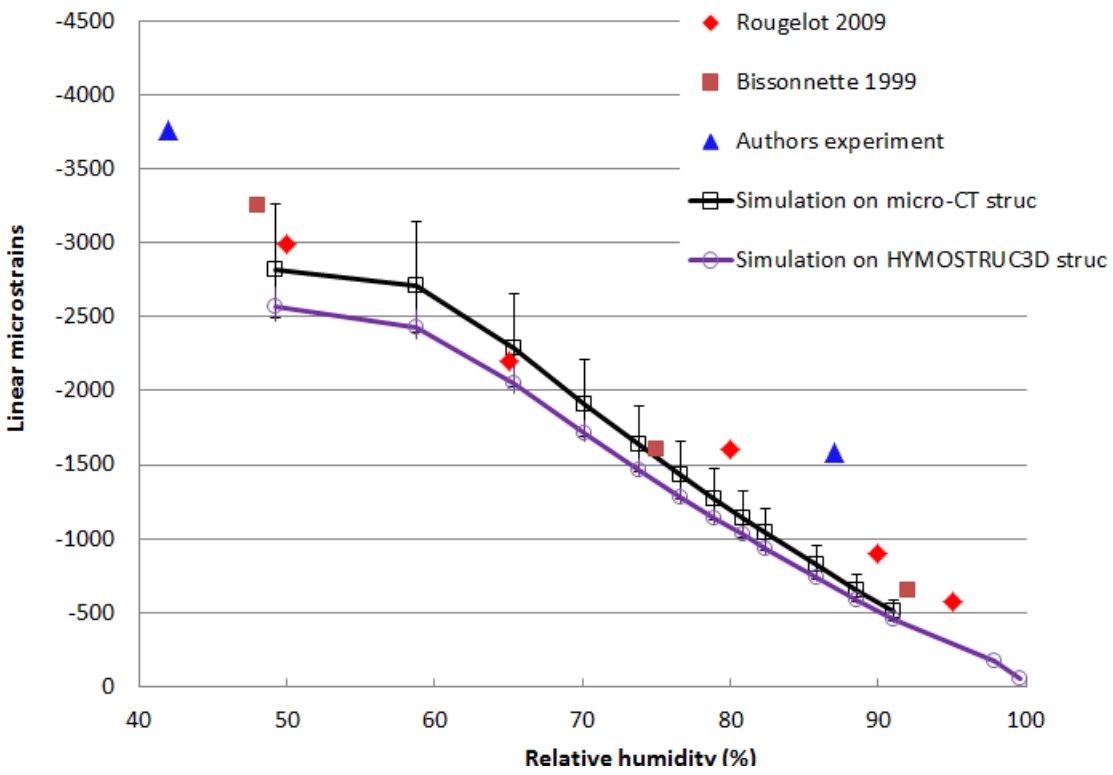

Figure 16: Drying deformation of cement paste (w/c=0.25, 28 days) by simulation and by experiments [1-2].

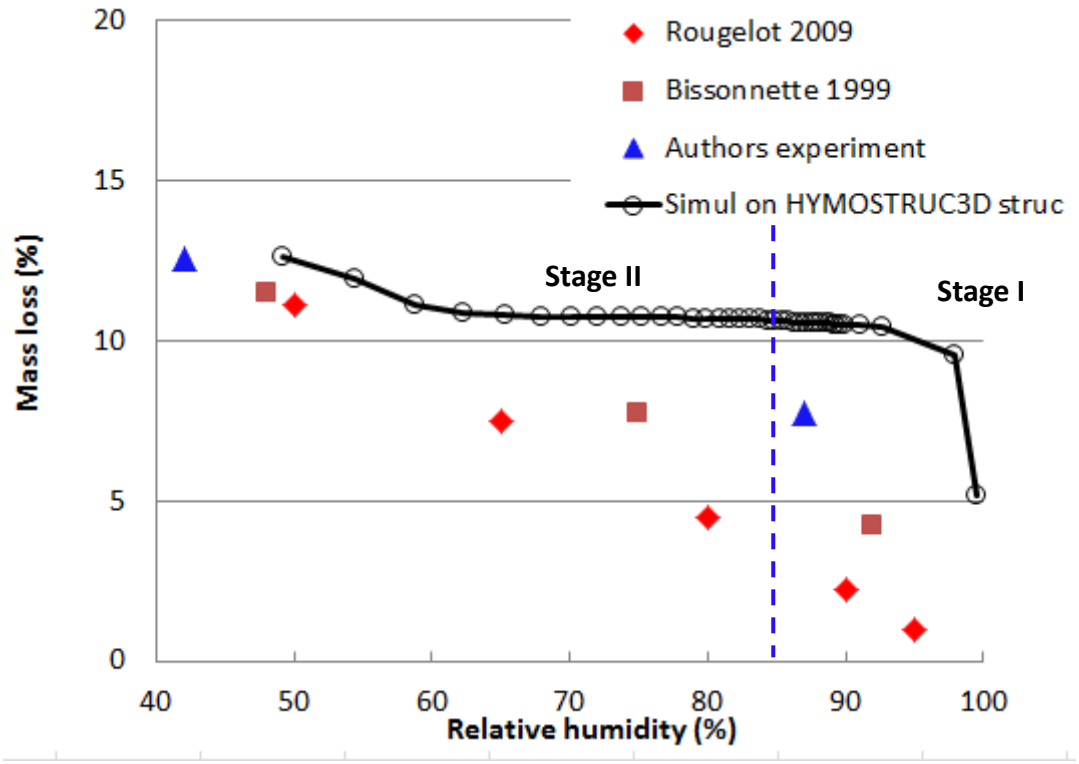

Figure 17: Weight loss of water in cement paste as RH decreases.

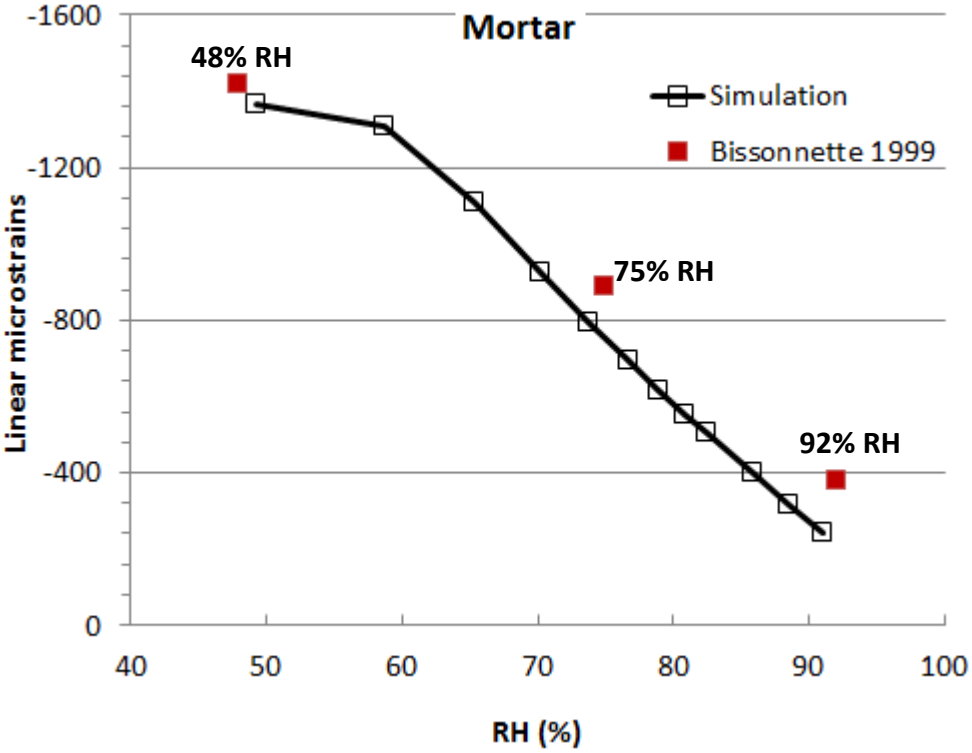

Figure 18: Drying deformation of mortar (V_{agg}=0.46; D_{max}=2.0 mm; D_{min}=0.2 mm) by simulation and by experiment [1].